

# Multi-modal AI for comprehensive breast cancer prognostication

Jan Witowski<sup>1</sup>, Ken Zeng<sup>1</sup>, Joseph Cappadona<sup>1</sup>, Jailan Elayoubi<sup>2</sup>, Elena Diana Chiru<sup>3</sup>,  
 Nancy Chan<sup>4</sup>, Young-Joon Kang<sup>5</sup>, Frederick Howard<sup>6</sup>, Irina Ostrovnaya<sup>7</sup>,  
 Carlos Fernandez-Granda<sup>8,9</sup>, Freya Schnabel<sup>4</sup>, Ugur Ozerdem<sup>4</sup>, Zoe Steinsnyder<sup>1</sup>,  
 Kangning Liu<sup>8</sup>, Nitya Thakore<sup>4</sup>, Mohammad Sadic<sup>4</sup>, Frank Yeung<sup>4</sup>, Elisa Liu<sup>4</sup>,  
 Theodore Hill<sup>4</sup>, Benjamin Swett<sup>4</sup>, Danielle Rigau<sup>4</sup>, Andrew Clayburn<sup>4</sup>, Valerie Speirs<sup>10</sup>,  
 Marcus Vetter<sup>3</sup>, Lina Sojak<sup>3</sup>, Simone Muenst Soysal<sup>11</sup>, Daniel Baumhoer<sup>11</sup>, Khalil Choucair<sup>2</sup>,  
 Yu Zong<sup>2</sup>, Lina Daoud<sup>2</sup>, Anas Saad<sup>2</sup>, Waleed Abdulsattar<sup>2</sup>, Rafic Beydoun<sup>2</sup>, Jia-Wern Pan<sup>12</sup>,  
 Haslina Makmur<sup>12</sup>, Soo-Hwang Teo<sup>12</sup>, Linda Ma Pak<sup>4</sup>, Victor Angel<sup>13</sup>,  
 Dovile Zilenaite-Petrulaitiene<sup>14</sup>, Arvydas Laurinavicius<sup>14</sup>, Natalie Klar<sup>4</sup>, Brian D. Piening<sup>15</sup>,  
 Carlo Bifulco<sup>15</sup>, Sun-Young Jun<sup>5</sup>, Jae Pak Yi<sup>5</sup>, Su Hyun Lim<sup>5</sup>, Adam Brufsky<sup>16</sup>,  
 Francisco J. Esteva<sup>17</sup>, Lajos Pusztai<sup>18</sup>, Yann LeCun<sup>8,9,19</sup>, and Krzysztof J. Geras<sup>1,8,4,✉</sup>

<sup>1</sup>Ataraxis AI

<sup>2</sup>Karmanos Cancer Institute

<sup>3</sup>Cancer Center Baselland

<sup>4</sup>NYU Grossman School of Medicine

<sup>5</sup>The Catholic University of Korea

<sup>6</sup>UChicago Medicine

<sup>7</sup>Memorial Sloan Kettering Cancer Center

<sup>8</sup>NYU Center for Data Science

<sup>9</sup>NYU Courant Institute of Mathematical Sciences

<sup>10</sup>The University of Aberdeen

<sup>11</sup>University Hospital Basel

<sup>12</sup>Cancer Research Malaysia

<sup>13</sup>Omica.bio

<sup>14</sup>Vilnius University

<sup>15</sup>Providence Health

<sup>16</sup>University of Pittsburgh Medical Center

<sup>17</sup>Northwell Health

<sup>18</sup>Yale School of Medicine

<sup>19</sup>Meta AI

✉krzysztof.geras@nyulangone.org

## Abstract

Treatment selection in breast cancer is guided by molecular subtypes and clinical characteristics. Recurrence risk assessment plays a crucial role in personalizing treatment. Current methods, including genomic assays, have limited accuracy and clinical utility, leading to suboptimal decisions for many patients. We developed a test for breast cancer patient stratification based on digital pathology and clinical characteristics using novel AI methods. Specifically, we utilized a vision transformer-based pan-cancer foundation model trained with self-supervised learning to extract features from digitized H&E-stained slides. These features were integrated with clinical data to form a multi-modal AI test predicting cancer recurrence and death. The test was developed and evaluated using data from a total of 8,161 breast cancer patients across 15 cohorts originating from seven countries. Of these, 3,502 patients from five cohorts were used exclusively for evaluation, while the remaining patients were used for training. Our test accurately predicted our primary endpoint, disease-free interval, in the five external cohorts (C-index: 0.71 [0.68-0.75], HR: 3.63 [3.02-4.37,  $p < 0.01$ ]). In a direct comparison (N=858), the AI test was more accurate than Oncotype DX, the standard-of-care 21-gene assay, with a C-index of 0.67 [0.61-0.74] versus 0.61 [0.49-0.73], respectively. Additionally, the AI test added independent information to Oncotype DX in a multivariate analysis (HR: 3.11 [1.91-5.09,  $p < 0.01$ ]). The test demonstrated robust accuracy across all major breast cancer subtypes, including TNBC (C-index: 0.71 [0.62-0.81], HR: 3.81 [2.35-6.17,  $p = 0.02$ ]), where no diagnostic tools are currently recommended by clinical guidelines. These results suggest that our AI test can improve accuracy, extend applicability to a wider range of patients, and enhance access to treatment selection tools.

## 1 Main

Over the past few decades, breast cancer treatment has evolved significantly with the introduction of various chemo, endocrine, and targeted therapies. Treatment selection is primarily guided by clinical guidelines that rely on clinicopathological factors such as tumor size, nodal status, and estrogen and HER2 receptor status. While this approach optimizes outcomes at the population level to a certain degree, it overlooks critical, actionable information for individual patients, exposing a significant gap in personalized care.

In an attempt to address this limitation, genomic assays were developed in the early 2000s, offering a more refined approach to patient risk stratification. Tools such as Oncotype DX [1], Mammaprint [2] and Prosigna [3] assess the risk of distant recurrence based on gene expression data. However, these assays were developed primarily for hormone receptor-positive (HR+) breast cancer patients, mainly to de-escalate adjuvant chemotherapy. In addition to being limited to certain cancer subtypes, their accuracy is modest, often on par with simple models based on clinical characteristics [4, 5]. These tests also require the processing of physical tissue specimens, which creates additional work for pathology departments and depletes tissue that could be used in the future for advanced molecular profiling.

Complementary to genomic assays, histopathological features are routinely evaluated by pathologists to stratify patient risk. These features include histologic grade, tumor infiltrating lymphocytes level, mitotic count, and Ki67 expression. It has been shown that these primarily morphological features add independent prognostic information to genomic scores, and recent prognostic models integrate both [6, 7]. However, these features are limited in their scope and prognostic ability, driving the need for stronger and more robust prognostic features. In recent years, advances in AI, particularly in self-supervised learning, have enabled the development of more effective methods for learning meaningful features from imaging data [8, 9, 10, 11, 12, 13]. These features are not based on pre-specified characteristics and extracting them does not require manual annotation by pathologists. Instead, AI models autonomously determine the most salient features by learning from millions of images. Early evidence shows that these AI-enabled features extracted from digital pathology images can be used to predict key patient characteristics and their long-term outcomes [14, 15, 16].

In response to the gaps in today’s treatment selection tools, we developed and evaluated an AI test for the stratification of invasive breast cancer patients. It is built upon the latest advances in self-supervised learning and digital pathology. Specifically, our test extracts strongly predictive morphological features from standard H&E-stained slides of core needle biopsy or surgical specimens utilizing *Kestrel* [17], a state-of-the-art pan-cancer AI foundation model. *Kestrel* is a variant of vision transformer [18] trained with self-supervised learning method DINOv2 [13] using 400M digital pathology image patches. The image patches used to train *Kestrel* were sourced from a large, heterogeneous database of pan-cancer whole slide images, including breast

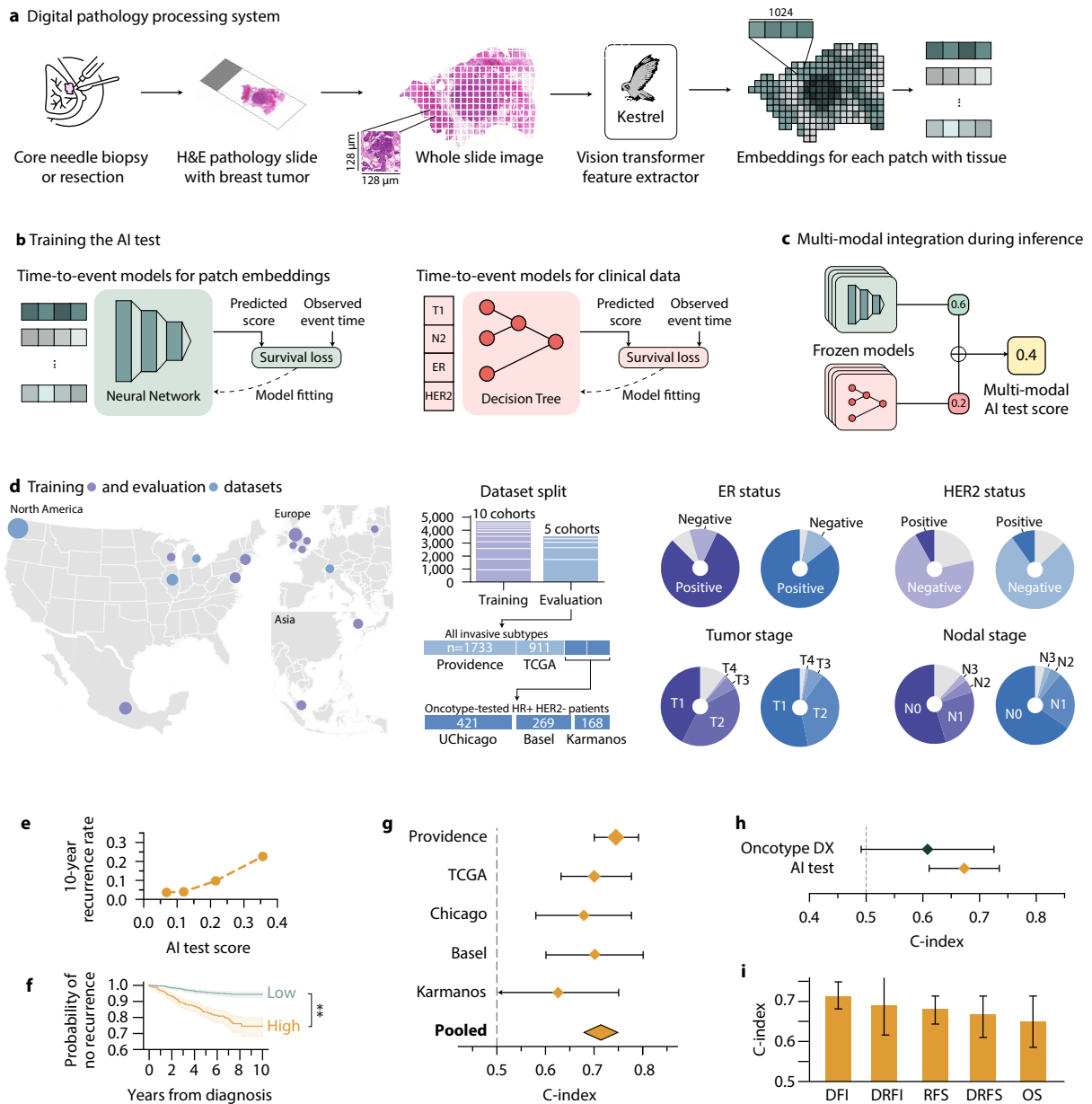


Figure 1: **We present a multi-modal AI test for invasive breast cancer.** **a**, The key component of the test is a system which processes high-resolution digital images of breast cancer specimens. Features are extracted from the digitized slides using *Kestrel*, a foundation model trained using self-supervised learning on a pan-cancer dataset of 400 million pathology image patches. **b**, Extracted pathology features and clinical features are used to train supervised time-to-event models predicting breast cancer recurrence or death. **c**, *The AI test* produces a multi-modal risk score, integrating pathological and clinical risk scores. **d**, We developed the AI test using 4,659 patients across 10 cohorts from six countries, and evaluated it on 3,502 patients from five patient cohorts which were not used during training. Evaluation sets consisted of two cohorts (Providence and TCGA) with all invasive breast cancer subtypes, and three cohorts (UChicago, Basel, and Karmanos) with only HR+ HER2- patients tested with Oncotype DX. **e**, Recurrence rate increases monotonically as the AI test score increases. **f**, Patients with predicted high risk had significantly worse outcomes compared to patients with predicted low risk. **g**, The AI test performed consistently across all evaluation datasets. **h**, In the direct comparison to a standard-of-care genomic assay, Oncotype DX, the AI test was a better predictor of cancer recurrence. **i**, The AI test performs consistently across various endpoints.

cancer images. Additionally, we tuned the hyperparameters for Kestrel using a novel search methodology that evaluates model performance on a suite of digital pathology benchmarks while iteratively scaling model and dataset size, yielding a model that is specially tuned for downstream tasks in digital pathology.

In this study, we present a multi-modal AI test that integrates pathology-based features, extracted by Kestrel, with routine clinical characteristics, namely cancer T and N stage, patient age, ER, PR and HER2 status and presence of ductal or lobular histology (Figure 1). The test produces a continuous score between 0 and 1 that is predictive of patient risk of cancer recurrence. The test was developed and evaluated using data from a total of 8,161 patients across 15 cohorts originating from seven countries. Of these, 3,502 patients from five cohorts were used exclusively for external evaluation, while the remaining patients were used for model training. Detailed patient characteristics are described in Table 1.

We evaluate our test’s prognostic capabilities in a variety of clinically meaningful patient groups. We also compare our test’s accuracy to a standard-of-care genomic assay, showing how the introduced multi-modal AI test enhances breast cancer prognostication.

## 2 Results

Unless explicitly stated otherwise, the presented results are from the multi-modal AI test. We first report its prognostic capability, i.e., whether our model accurately predicts the risk of cancer recurrence and distinguishes between high- and low-risk patients. Then, we compare its accuracy against a standard-of-care genomic risk signature in various molecular, histological and clinical subgroups. Finally, we discuss potential clinical use cases. When reporting performance across multiple datasets, we present pooled results, using a random effects model (see Appendix A.7 and A.6 for performances on individual datasets).

To evaluate how well the test orders patients according to their risk, we report the concordance index (C-index), a metric analogous to AUROC which can be computed for censored outcomes. Additionally, we estimate the hazard ratio (HR) for the AI test in univariate and multivariate Cox proportional hazards models. The hazard ratio is estimated from the continuous score for every 0.2 unit increase in our score. Unless explicitly stated otherwise, we use the continuous AI test risk score, rather than its dichotomized version. Refer to Methods (Section 4) for a detailed explanation of the performance metrics used in this paper.

### 2.1 The AI test is predictive of breast cancer recurrence and survival

The AI test was found to be prognostic in all five patient cohorts used as external evaluation sets. For the primary endpoint, disease-free interval (DFI), the risk score generated by our model achieved a pooled C-index of 0.71 [0.68-0.75] and a pooled HR of 3.63 [3.02-4.37,  $p<0.01$ ].

Two of the test datasets, Providence and TCGA-BRCA, represent a broad spectrum of invasive breast cancer patients. For prediction of DFI, our AI test achieved a C-index of 0.74 [0.70-0.79] and a HR 4.02 [3.09-5.23,  $p<0.01$ ] in the Providence cohort (N=1,733), and a C-index of 0.70 [0.63-0.77] and a HR of 3.00 [2.10-4.28,  $p<0.01$ ] in the TCGA-BRCA cohort (N=911).

Three cohorts — Karmanos, Basel, and UChicago — included only HR+ HER2– patients who were previously tested with Oncotype DX. The AI test achieved a C-index of 0.62 [0.49-0.75] and a HR of 3.82 [1.33-10.98,  $p=0.01$ ] in the Karmanos cohort (N=168), a C-index of 0.70 [0.60-0.80] and a HR of 3.98 [1.92-8.25,  $p<0.01$ ] in the Basel cohort (N=269), and a C-index of 0.67 [0.58-0.77] and a HR of 3.25 [1.45-7.31,  $p<0.01$ ] in the UChicago cohort (N=421).

The AI test was also prognostic for secondary endpoints. In analyses utilizing random effects models, pooled C-indices and HRs were as follows. For distant-disease free interval (DRFI), the test achieved a C-index of 0.70 [0.61-0.78] and a HR of 4.02 [2.64-6.13,  $p<0.01$ ]. For overall survival (OS), the test achieved a C-index of 0.65 [0.58-0.72] and a HR of 2.52 [1.88-3.38,  $p<0.01$ ]. For recurrence-free survival (RFS), the test achieved a C-index of 0.68 [0.65-0.71] and a HR of 2.65 [2.33-3.01,  $p<0.01$ ]. And for distant recurrence-free survival (DRFS), the test achieved a C-index of 0.66 [0.61-0.71] and a HR of 2.64 [2.14-3.26,  $p<0.01$ ]. Forest plots for all endpoints and metrics are reported in Appendix A.6, and endpoints are defined in Appendix A.4.

## 2.2 The AI test is more accurate than a genomic assay in predicting cancer recurrence in HR+ patients

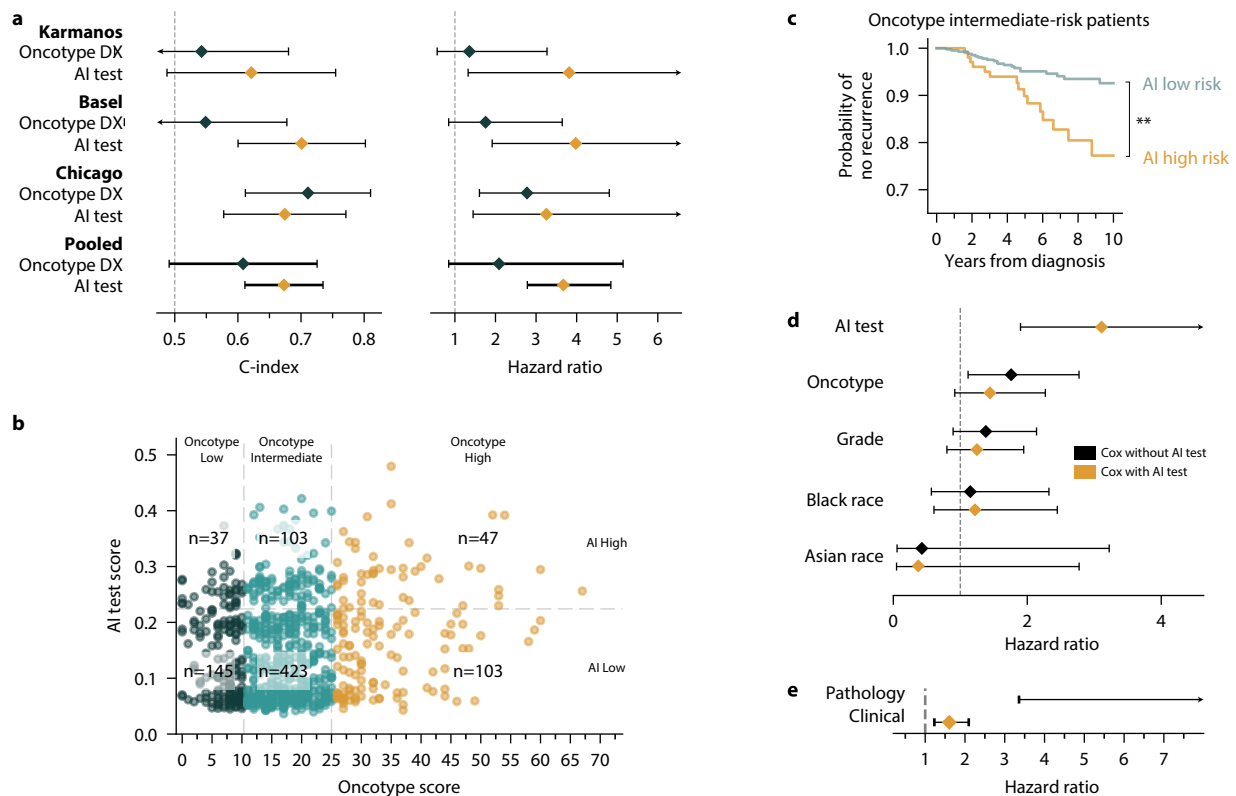


**Figure 2: The AI test reclassifies patients tested with a standard-of-care genomic assay into different risk categories.** Oncotype DX, a standard-of-care 21-gene assay, classifies patients into low-, intermediate-, and high-risk groups. The AI test demonstrated statistically significant discrimination between high- and low-risk patients without the need to introduce an intermediate-risk group, thereby enhancing clarity in decision-making. We analyze the differences in classification and patient outcomes between the two tests using data from the Karmanos, Basel, and UChicago cohorts. **a**, Comparison of prognostic ability between Oncotype DX and the AI test in univariate models. **b**, A scatter plot illustrating risk scores for Oncotype DX-tested patients. Each point represents one patient. The majority of patients with intermediate Oncotype DX scores were reclassified into the low-risk group by the AI test. **c**, For intermediate-risk Oncotype DX patients, the AI test was able to accurately distinguish between low- and high-risk patients. **d**, The AI test is significantly associated with a disease-free interval after adjusting for Oncotype DX score, grade and race in a multivariate Cox regression model. **e**, Comparing the AI test’s modalities in a multivariate Cox model shows that the pathology score was more informative than the clinical score within the Oncotype DX cohort.

We compared the prognostic performance and potential clinical utility of our model to Oncotype DX, a standard-of-care 21-gene assay developed to predict distant recurrence risk. Three external cohorts (Karmanos, Basel, UChicago) contain a total of 858 patients who were tested with Oncotype DX Recurrence Score assays performed as part of routine care. Full results are in Appendix A.8.

In the Karmanos cohort, the AI model’s C-index for DFI was 0.62 [0.49-0.76] and the HR was 3.81 [1.33-10.98,  $p < 0.01$ ], compared with Oncotype DX’s C-index of 0.54 [0.41-0.68] and HR of 1.36 [0.56-3.27,  $p = 0.50$ ]. In the Basel cohort, the AI test’s C-index was 0.70 [0.60-0.80] and the HR was 3.37 [1.54-7.40,  $p < 0.01$ ], compared with Oncotype DX’s C-index of 0.55 [0.42-0.68] and HR of 1.76 [0.85-3.64,  $p = 0.13$ ]. In the UChicago cohort, the AI test’s C-index was 0.67 [0.58-0.77] and the HR was 3.26 [1.45-7.31], compared with Oncotype DX’s C-index of 0.71 [0.61-0.81] and HR of 2.78 [1.61-4.81]. Together, the AI test achieved a pooled C-index of 0.67 [0.61-0.74] and HR of 3.67 [2.79-4.84,  $p < 0.01$ ], compared to Oncotype DX’s C-index of 0.608 [0.491-0.725] and HR of 2.09 [0.85-5.15,  $p = 0.21$ ]. These comparisons are illustrated in Figure 2A.

Oncotype DX has been shown to predict the benefit of adjuvant chemotherapy in HR+ patients. Patients

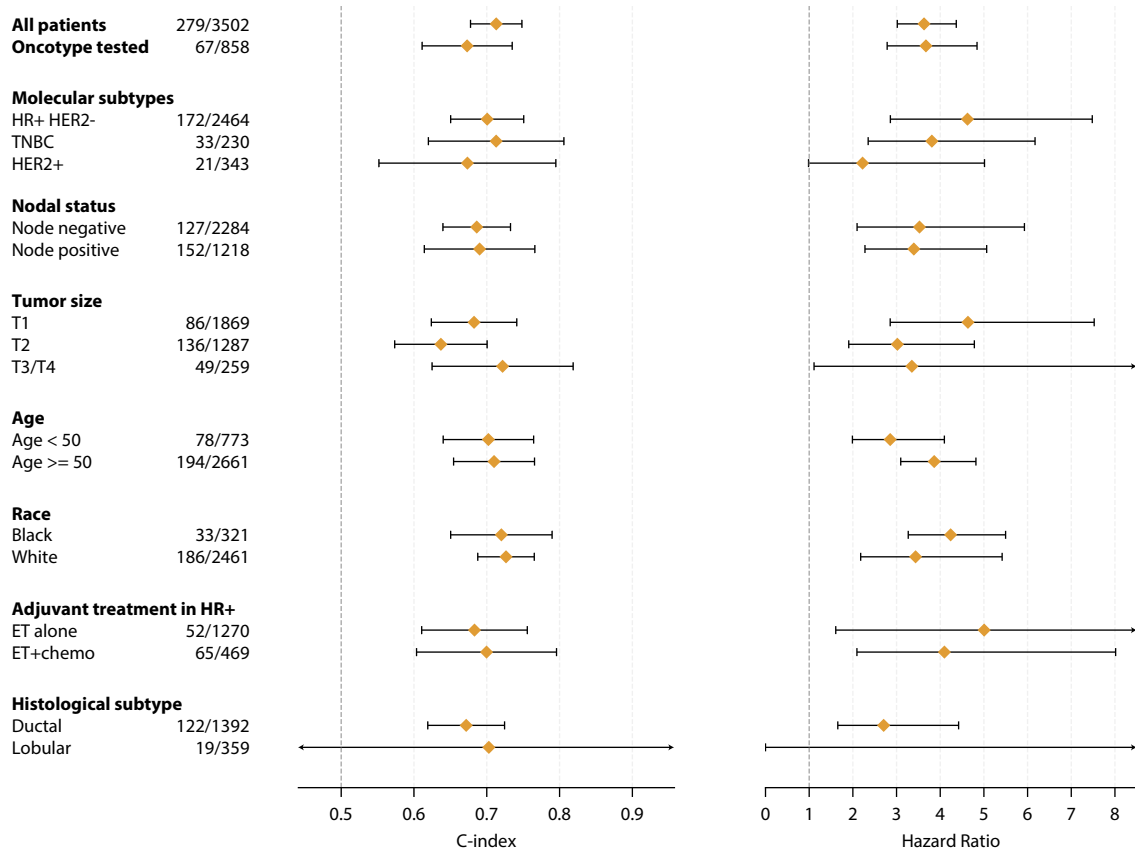
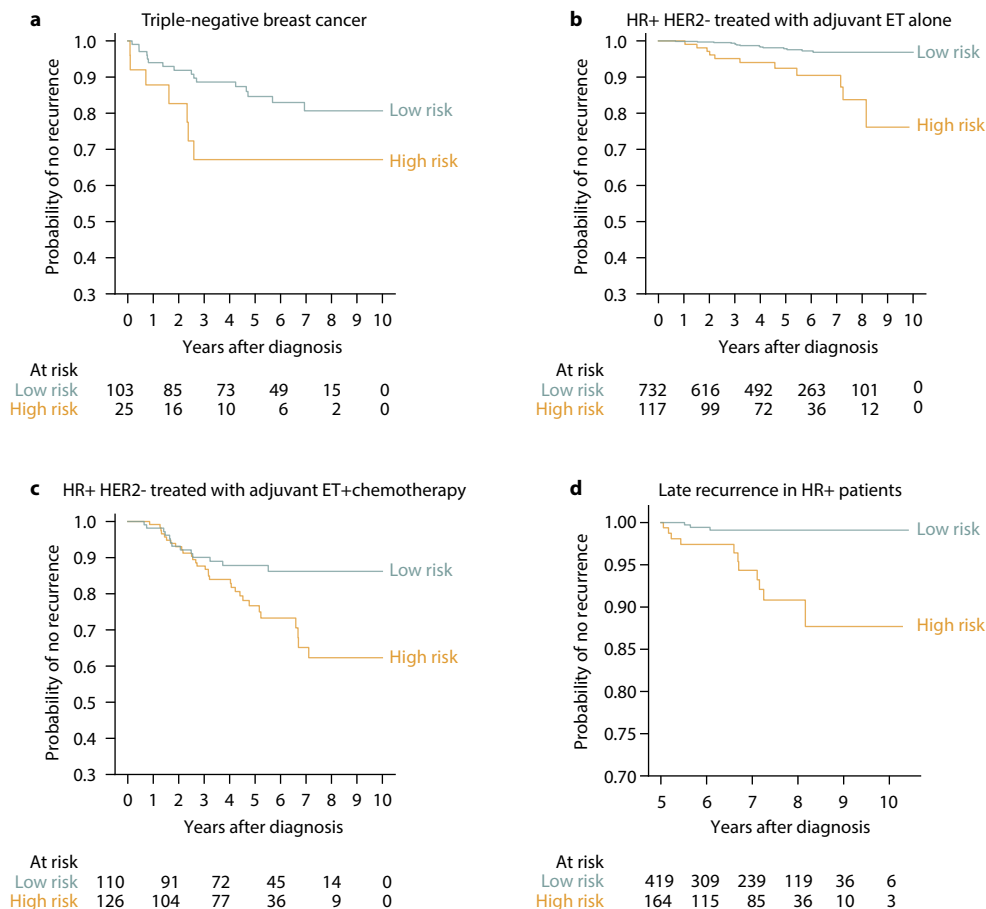


Figure 3: **The AI test performs well in all major clinically relevant groups.** Forest plots display our AI test’s performance across clinical, molecular, and demographic groups. Next to each group name we report the number of disease-free interval events and total number of patients. Subgroup performances were pooled across all evaluation cohorts using a random effects model.

with high Oncotype DX scores had significant chemotherapy benefits, while patients with low Oncotype DX scores did not [19]. Large randomized clinical trials, TAILORx [20] and RxPONDER [21], have shown that some patients with intermediate Oncotype DX scores might also safely avoid adjuvant chemotherapy. For patients tested with Oncotype DX, the AI model would re-classify 666 out of 858 (77.6%) patients into different risk categories (Figure 2B). All intermediate Oncotype-risk patients (61.3% of all Oncotype DX patients) would be reclassified as either low- or high-risk by our AI test. 423 out of 526 (80.4%) intermediate Oncotype-risk patients would be classified as low-risk patients and 103 of 526 (19.6%) as high-risk patients using the AI test. Notably, 103 high Oncotype-risk patients (12.0% of all Oncotype DX patients) would be reclassified as low-risk by the AI test. Within this intermediate Oncotype-risk group, the continuous AI test score was significantly associated with recurrence (HR: 3.45 [1.85-6.42,  $p < 0.01$ ]) in the Karmanos, Basel and UChicago cohorts after adjusting for the dataset (see Table 5).

Finally, we demonstrate that the AI test provides independent prognostic value alongside Oncotype DX as well as other common clinical indicators. To do this, we incorporated the AI test score into a multivariate Cox proportional hazards model along with Oncotype DX score, age, Nottingham cancer grade, dataset and race. Dataset was accounted for with an indicator variable for Karmanos and Chicago, with Basel as the reference dataset. Race was accounted for with an indicator variable for Other/Unknown, Asian, and Black, with White as the reference group. After adjusting for these factors, the AI test achieved a HR of 3.11 [1.91-5.09,  $p < 0.01$ ]. In comparison, Oncotype DX achieved a HR of 1.47 [0.93-2.30,  $p = 0.10$ ], which is not statistically significant. The HR between Karmanos and Basel was 0.91 [0.35-2.41,  $p = 0.85$ ], which is not significant. The hazard ratio between Chicago and Basel was 0.30 (0.09-1.00,  $p = 0.05$ ). None of the hazard ratios associated with race were significant. The full results are in Table 6 in Appendix A.5.

## 2.3 The AI test performs well in various clinically meaningful subgroups. Potential clinical utility.



**Figure 4: The AI test is prognostic in clinically meaningful situations.** **a**, In triple-negative breast cancer, there is an ongoing discussion about potential strategies to de-escalate the KEYNOTE-522 regimen, for example with shorter or anthracycline-free chemotherapy regimens or complete omission of adjuvant treatment. While some biomarkers, such as tumor-infiltrating lymphocytes, are associated with long-term outcomes and pathological complete response, there is still a need for a more robust assessment of systemic therapy benefits. **b-d**, In hormone receptor-positive patients, questions about treatment selection involve the addition of adjuvant chemotherapy, extended endocrine therapy (ET), and new agents, such as CDK4/6 inhibitors. We hypothesize that high-risk HR+ patients who received adjuvant ET alone (**b**) might benefit from the addition of chemotherapy, and high-risk HR+ patients who received chemoendocrine therapy (**c**) might benefit from the addition of CDK4/6 inhibitors. Finally, HR+ patients who received five years of adjuvant endocrine therapy (**d**) are candidates for extended endocrine treatment. A few assays have been shown to be associated with late recurrence and predict the benefit of extended endocrine therapy [22]. All plots in this figure are for the Providence cohort (the largest evaluation cohort).

Traditional genomic assays are typically developed for specific patient subgroups, such as Oncotype DX for HR+ HER2- patients, and cannot be used in patients with less common molecular, histological, or clinical characteristics. Given that the AI test was developed using data from non-metastatic breast cancer patients without additional exclusion criteria, we can evaluate its prognostic accuracy in various subgroups. This includes patients with varying age and menopausal status, nodal status, tumor size, estrogen and HER2 receptor status, race, and administered of adjuvant therapy (Figure 3). Furthermore, our analysis indicates that the test score is consistent with known clinical factors that influence cancer prognosis, including higher scores in ER- and PR- patients, as well as patients with more advanced staging (both N and T) (Figure 5).

Currently, there is no prognostic/predictive tool supported by NCCN guidelines for use in triple-negative

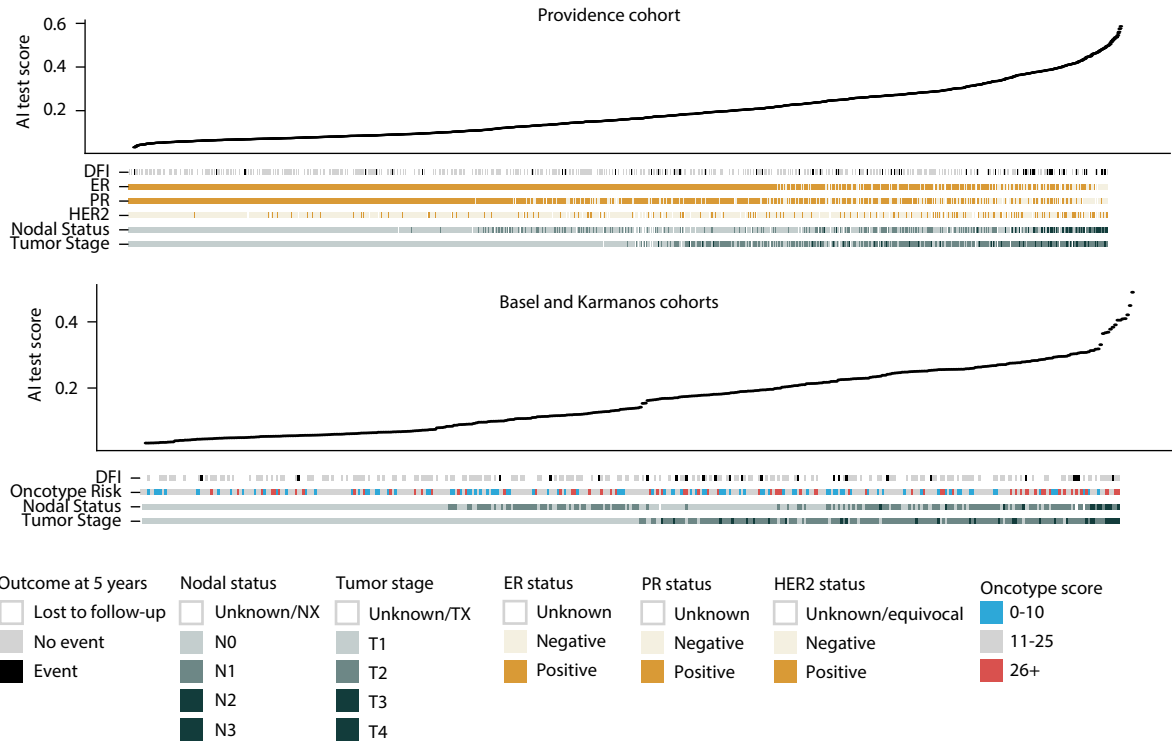


Figure 5: **Relationship between predicted risk of recurrence and established prognostic factors.** The top plot analyzes the Providence cohort with all invasive breast cancer subtypes to display the relationship with the ER/HER2 status. The bottom plot combines the Basel and Karmanos cohorts and illustrates the Oncotype score in relationship with the AI test score. Higher scores are observed in patients with HR– and HER2+ status and in patients with more advanced disease.

and HER2+ breast cancer patients [23]. The AI test reliably predicted DFI in TNBC (N=230, C-index: 0.71 [0.62-0.81], HR: 3.81 [2.35-6.17, p=0.02]) and HER2+ patients (N=343, C-index: 0.67 [0.55-0.80], HR: 2.22 [0.99-5.01, p=0.05]).

NCCN guidelines also do not currently recommend any tests for the selection of adjuvant systemic therapy in most premenopausal HR+ patients (intermediate-risk node-negative and low- or intermediate-risk 1-3 LN+). The AI test reliably predicted DFI in HR+ premenopausal patients (if the menopausal status is unknown, we consider patients younger than 50 years as premenopausal), with a C-index of 0.655 [0.583-0.726] and a HR of 2.87 [1.81-4.55, p<0.01] (N=677).

Furthermore, genomic assays have been reported to perform poorly in Black patients [24, 25]. The AI test reliably predicted DFI in Black patients (N=299), with a C-index of 0.720 [0.65-0.79] and a HR 4.24 [3.27-5.50, p<0.01]. Among White patients (N=2,461), the AI test achieved a C-index of 0.73 [0.69-0.79] and a HR of 3.44 [2.18-5.42, p<0.01].

Some prognostic genomic assays, including Oncotype DX, have also been shown to be predictive of adjuvant chemotherapy benefit [19, 26] in HR+ patients. We hypothesize that our test can identify patients who might benefit from adjuvant chemotherapy, CDK4/6 inhibitors, and extended endocrine therapy.

First, the AI test was prognostic in HR+ HER2– patients who received adjuvant endocrine therapy (ET) alone (N=1171, C-index: 0.68 [0.61-0.76], HR: 5.01 [1.61-15.58, p=0.03]). High-risk patients in the ET group are likely to benefit from the addition of adjuvant chemotherapy.

Second, the AI test was prognostic in HR+ HER2– patients who received adjuvant chemoendocrine therapy (N=469, C-index: 0.70 [0.60-0.80], HR: 4.10 [2.09-8.02, p<0.01]). Patients who still have “residual” high risk while receiving both endocrine and chemotherapy are likely to benefit from the addition of CDK4/6 inhibitors.

Finally, the AI test was prognostic for late recurrence in HR+ HER2– patients (N=1158, C-index 0.79

[0.71-0.86], HR 8.44 [3.11-22.93,  $p < 0.01$ ]), suggesting that patients with high risk of cancer recurrence after 5 years might benefit from extended endocrine therapy.

To illustrate how our test can be used for clinical decision making in these subgroups, we defined high- and low-risk groups using the 80<sup>th</sup> percentile cutoff from our largest internal training dataset (it was giving us HR with significant p-value and similarly balanced high- and low-risk groups in all subgroups), verifying that high-risk patients have worse outcomes than low-risk patients. We apply this cutoff to the Providence cohort and compare outcomes between the low- and high-risk groups (Figure 4).

### 3 Discussion

In this study, we present a novel prognostic multi-modal AI test for invasive breast cancer. The overall performance of our test is robust across breast cancer patients. The test also outperformed Oncotype DX in three cohorts — Karmanos, Basel, and UChicago. Notably, the presented test is one of the few prognostic tools that have been clinically validated in triple-negative and HER2+ breast cancer patients. This capability, combined with strong performance regardless of nodal status and patient age, supports the viability of the AI test as a single tool to inform treatment decisions in all breast cancer patients.

The proposed AI test is designed to predict cancer recurrence risk, similar to genomic assays such as Oncotype DX and MammaPrint. However, just like these assays, it is not explicitly trained to model treatment effects. We expect that when validated using randomized prospective data, our prognostic test will show predictive capabilities in the same manner that the genomic assays do. That is, high-risk patients will benefit from more aggressive treatment options (such as adjuvant chemotherapy), while low-risk patients will have no benefit. While this study uses observational data and did not evaluate the test’s predictive capabilities (i.e., its ability to determine whether a patient is likely to benefit from a specific treatment), we present several potential clinical implications of using such a test in a clinical setting.

The AI test has the potential to refine clinical decision-making in several key areas. In HR+ patients who are candidates for adjuvant chemotherapy, the AI test was more accurate than Oncotype DX. This can potentially improve the selection of patients who can benefit from chemotherapy in addition to endocrine therapy. In a multivariate analysis, the AI test was shown to add independent prognostic information with respect to Oncotype and cancer grade, which indicates that it captures information that is strongly predictive and independent from existing clinical factors. Importantly, the AI test was prognostic in premenopausal HR+ patients, expanding patient groups who could be evaluated for cancer recurrence risk. Finally, we show that the AI test is prognostic in HR+ patients who received adjuvant chemoendocrine therapy, and identifies patients with high “residual” recurrence risk. We hypothesize that these patients might benefit from adjuvant CDK4/6 inhibitors. This use case is especially meaningful given recent FDA approval for ribociclib, which can be used in a wide group of HR+ patients, including node-negative cases. Identifying high-risk patients beyond basic clinical characteristics will be important in selecting patients who would benefit from CDK4/6 inhibitor treatment.

Besides HR+ patients, the test was prognostic in triple-negative and HER2+ patients, for which there are no NCCN guideline-supported tests for treatment selection. Current standard of care treatment in triple-negative breast cancer involves intense immunochemotherapy (KEYNOTE-522 regimen [27, 28]). There are multiple ongoing clinical trials working on treatment de-escalation through avoiding adjuvant pembrolizumab in patients with pathological complete response (OptimICE-pCR [29, 30]) or using shorter, anthracycline-free neoadjuvant chemotherapy regimen in patients with immune-enriched TNBC (NeoTRACT) [31].

The AI test was developed using Kestrel, an AI foundation model for digital pathology trained to extract morphological features from digitized pathology slides. Kestrel differs from the previous generation of feature extractors for digital pathology which relied on pre-specified “pathomic” features [32]. Kestrel, on the other hand, was trained with self-supervised learning, which does not require any pre-specification of features; rather, the self-supervised learning paradigm enables the model to learn the most salient features. While this sacrifices a priori explainability, the model can still be explained post hoc. Finally, because Kestrel was developed using a pan-cancer dataset, it can easily be applied to other clinical indications.

Applying self-supervised learning to develop prognostic/predictive models is an emerging research area. Spratt et al. demonstrated successful application of this approach to prostate cancer in a series of publications [33, 34]. The prostate test has been developed and validated using several randomized clinical

trials. Garberis et al. developed an AI test for breast cancer based on morphological features extracted with contrastive learning which showed positive results [35]. However, that study was limited to standalone evaluation on a single ER+ HER2- patient cohort. Volinsky-Fremond et al. applied a self-supervised deep learning models to H&E-stained endometrial tumor slides, demonstrating performance superior to the current gold standard of combined pathological and molecular analysis, additionally finding their test predictive of chemotherapy benefit in the PORTEC-3 trial [36].

There are several analyses that we hope to carry out in the future to address potential limitations of this analysis. Most importantly, this study used retrospective observational data, which is not suitable for the evaluation of predictive capabilities. Also, the observational data may be biased given the small sample sizes of some cohorts. We mitigate this potential bias by analyzing several external datasets.

Integration of digital pathology-based tests into clinical workflow offers several advantages over genomic and other molecular prognostic and predictive tests. First, the turnaround time is significantly shorter, potentially allowing for more timely treatment decisions. Second, by utilizing standard H&E-stained slides and not requiring specialized wet lab tissue processing, the test is likely to be substantially cheaper than genomic assays, improving access to treatment selection testing in resource-limited settings. Third, our test can be performed on core biopsy slides, which allows for earlier risk assessment and might inform neoadjuvant therapy decisions. Finally, this digital approach preserves valuable tumor samples, which might be needed for deep sequencing in cases of disease progression.

## 4 Methods

### 4.1 Data

To execute this project we assembled a diverse collection of both public datasets (TCGA-BRCA [37, 38], METABRIC [39], BASIS [40]) and private datasets from several sources (NYU Langone Health, The Catholic University of Korea, Gundersen Health, National Center of Pathology in Lithuania, Breast Cancer Now Biobank, Cancer Research Malaysia, Omica.bio Cancer Atlas, Wales Cancer Biobank, Karmanos Cancer Institute, University Hospital Basel, and UChicago Medicine). All together we have 5162 slides from 4659 patients across 10 datasets for training, and 3632 slides from 3502 patients from 5 datasets for evaluation. This represents one of the largest data collection efforts for the purpose of predicting breast cancer recurrence. The breakdown of patient demographic, molecular, and clinical characteristics is described in Table 1.

### 4.2 Task and evaluation

Our primary task was to accurately predict the risk of cancer-related events. To accomplish this, we trained time-to-event models using clinical variables and digital pathology slides. For both modalities, we trained several models and ensembled their predictions, as detailed in Section 4.3.1. We then created a multi-modal model by averaging predictions of the two ensembles. We trained and evaluated the models using the definitions of endpoints in Table 3.

#### 4.2.1 Performance metrics

Time-to-event models can be evaluated using a few different metrics that highlight various aspects of their performance. The two primary metrics we use are the concordance index (C-index) and hazard ratio (HR). Additionally, as we used several different datasets for evaluation, we aggregated results using random effects models. We refer to such aggregated metrics as *pooled*. In the following paragraphs, we justify the use of these metrics in our application. Detailed explanations of how the metrics are computed are in the Appendix.

**C-index.** To evaluate the prognostic ability of our model, we used the concordance index (C-index). The C-index measures how well the predicted risk ranking of patients aligns with the actual order in which they experienced events. A C-index of 1.0 indicates that patients are perfectly ordered according to predicted risk, whereas a C-index of 0.5 suggests that the model’s ordering is no better than random. The advantage of the C-index is that it is easy to interpret, as it analogous to AUROC in how it is computed, while accommodating censoring. A detailed explanation of how the C-index is computed is in Appendix A.1.

**Hazard ratio for a continuous score.** For a continuous score, the hazard ratio represents the relative increase or decrease in the risk of the event associated with a one-unit increase in that score. In other words, it quantifies how changes in the score influence the relative risk of the event happening over time. In our analysis, we compare a 0.2 unit increase in our score (which ranges from 0 to 1) to a 20 unit increase in the Oncotype score (which ranges from 0 to 100). A detailed explanation of how the hazard ratio is computed is in Appendix A.2.

**Hazard ratio for a dichotomized score.** For a dichotomized score, the patients are stratified into two categories: high-risk and low-risk. The hazard ratio assesses the relative risk of experiencing an event in the two categories. For example, a HR of 2 indicates that the high-risk group is twice as likely to experience the event compared to the low-risk group. Hazard ratios come with associated p-values, computed with the Wald test, that evaluate whether the estimated hazard ratio for each covariate is statistically significantly different from 1.

**Multivariate Cox proportional hazards model.** To assess the simultaneous impact of multiple variables on the outcome, we fit a multivariate Cox proportional hazards model with all the variables of interest. The Cox regression coefficients estimate the strength of association between each variable and the outcome, adjusted for other covariates. A coefficient greater than zero, or a hazard ratio exceeding 1 (as determined by

Table 1: Datasets used for training and evaluation. All values are N (%) unless indicated otherwise.

Category	Training cohorts (N=4,659)	Evaluation cohorts (N=3,502)
<b>Age median, [IQR]</b>	58 [49-68]	60 [51-68]
<b>Follow-up time median, [IQR]</b>	5.11 [3.62-8.31]	4.51 [2.42-7.15]
<b>ER receptor status</b>		
Positive	3748 (80.45%)	2992 (85.44%)
Negative	540 (11.59%)	399 (11.39%)
Unknown	371 (7.96%)	111 (3.17%)
<b>PR receptor status</b>		
Positive	2676 (57.44%)	2648 (75.61%)
Negative	1010 (21.68%)	728 (20.79%)
Unknown	973 (20.88%)	126 (3.60%)
<b>HER2 receptor status</b>		
Positive	377 (8.09%)	348 (9.94%)
Negative	3286 (70.53%)	2702 (77.16%)
Equivocal or Unknown	996 (21.38%)	452 (12.91%)
<b>T stage</b>		
T1	1880 (40.35%)	1869 (53.37%)
T2	1780 (38.21%)	1287 (36.75%)
T3	252 (5.41%)	225 (6.42%)
T4	51 (1.09%)	40 (1.14%)
Unknown/TX	464 (9.96%)	81 (2.31%)
<b>N stage</b>		
N0	2550 (54.73%)	2284 (65.22%)
N1	1174 (25.20%)	839 (23.96%)
N2	251 (5.39%)	156 (4.45%)
N3	141 (3.03%)	86 (2.46%)
Unknown/NX	543 (11.65%)	137 (3.91%)
<b>Ductal histology</b>		
Yes	3567 (76.56%)	1392 (39.75%)
No	904 (19.40%)	377 (10.77%)
Unknown	188 (4.04%)	1733 (49.49%)
<b>Lobular histology</b>		
Yes	600 (12.88%)	359 (10.25%)
No	3871 (83.09%)	1410 (40.26%)
Unknown	188 (4.04%)	1733 (49.49%)
<b>Any recurrence</b>		
Yes	726 (15.58%)	279 (7.97%)
No	3933 (84.42%)	3223 (92.03%)
<b>Distant recurrence</b>		
Yes	457 (9.81%)	174 (4.97%)
No	4098 (87.96%)	3328 (95.03%)
Unknown	104 (2.23%)	0 (0.00%)
<b>Death</b>		
Yes	935 (20.07%)	303 (8.65%)
No	3710 (79.63%)	3199 (91.35%)
Unknown	14 (0.30%)	0 (0.00%)
<b>Adjuvant chemo- and endocrine therapy</b>		
Chemoendocrine therapy	1124 (24.13%)	768 (21.93%)
Chemotherapy only	564 (12.11%)	500 (14.28%)
Endocrine therapy only	1551 (33.29%)	1442 (41.18%)
Unknown	729 (15.65%)	368 (10.51%)

the Wald test), suggests a positive association between the variable and the outcome after accounting for the influence of other factors. This analysis allows us to estimate the hazard ratio associated with different features after adjusting for the varying patient outcome distributions of different datasets. This analysis is performed to validate the association between our test and recurrence, even after adjusting for established prognostic factors such as cancer grade and Oncotype DX score. This analysis is used to assess whether our pathology model provides prognostic information independent of the clinical model.

**Recurrence rate as a function of the AI test score.** To assess how the AI test score corresponds to patient recurrence, we divided patients based on their AI test scores into groups using quartiles. We then used the Kaplan-Meier estimator to compute 10-year recurrence rates (with confidence intervals) across these groups of patients. The aim was to compare the average score within each group to the estimated recurrence rate within that group. This approach helped us evaluate how well the AI test score corresponded to the observed risk of recurrence, providing a clear way to assess whether higher test scores consistently correspond to higher recurrence rates.

#### 4.2.2 Hyperparameter selection

In all instances, we selected the hyperparameters of the models through random search [41]. Unless otherwise explicitly stated we maximized the C-index. As we were tuning relatively few hyperparameters with moderately wide intervals, random search explores the hyperparameter space sufficiently well.

For pathology data, the performance of the models sampled in the hyperparameter search were estimated using modified multiple-source cross-validation [42]. That is, we had two sets of datasets  $\mathcal{D}^T = \{D_1, D_2, \dots, D_J\}$  and  $\mathcal{D}^V = \{D_{J+1}, D_{J+2}, \dots, D_{J+K}\}$ . Datasets in  $\mathcal{D}^T$  were reserved only for training, while  $\mathcal{D}^V$  could be used for training or validation. For a given hyperparameter setting, we trained  $K$  models,  $m_1, m_2, \dots, m_K$ . The training set for the  $k^{\text{th}}$  model was  $\mathcal{D}_k^T = \mathcal{D}^T \cup \mathcal{D}^V \setminus D_{J+k}$ , and the validation set was  $D_{J+k} \in \mathcal{D}^V$ . The performances on the validation sets were averaged, weighted by the number of comparisons  $c_k$  used in the computation of the validation C-index using the dataset  $D_{J+k}$ . This procedure was used for performance estimation and hyperparameter selection as formalized in Algorithm 1.

---

**Algorithm 1** Multiple-source cross-validation for pathology models

---

```

for n = 1 to N do
  Sample hyperparameters  $\theta_n$ 
  for k = 1 to K do
    Train a model  $m_k^{\theta_n}$  using data  $\mathcal{D}^T \cup \mathcal{D}^V \setminus D_{J+k}$ 
    Evaluate the model  $m_k^{\theta_n}$  using  $D_{J+k}$  to obtain the validation performance  $v_k^{\theta_n}$ 
  end for
  The overall validation score of hyperparameters  $\theta_n$  is  $v^{\theta_n} = \frac{1}{K} \sum_{k=1}^K c_k v_k^{\theta_n}$ .
  The model obtained for  $\theta_n$  is  $m^{\theta_n} = \frac{1}{K} \sum_{k=1}^K m_k^{\theta_n}$ .
end for
Select the hyperparameters  $\theta_n^*$  yielding the best overall validation score.

```

---

In practice, to limit the variance in hyperparameter selection, for each set of hyperparameters, we trained and evaluated several models with different random seeds and averaged the validation performances.

In our implementation, when training the pathology models, we set  $\mathcal{D}^T = \{\text{Korea, Gundersen, Lithuania, BCN, Malaysia, Karmanos, Basel, METABRIC, BASIS}\}$  and  $\mathcal{D}^V = \{\text{NYU, Omica, Wales}\}$ .

As clinical models use a much lower dimensional input than pathology models and exhibit less variance, we adopted a simpler cross-validation procedure. We divided the data into  $k$  splits, that is,  $\mathcal{D}^C = \{D_1^C, D_2^C, \dots, D_K^C\}$ . For each iteration, we trained the models using  $\mathcal{D}^C \setminus D_k^C$  and selected the hyperparameters that performs the best for this split based on validation performance on  $D_k^C$ . This procedure was used for performance estimation and hyperparameter selection as formalized in Algorithm 2.

In our implementation, when training the clinical models, we trained using three splits  $\mathcal{D}^C = \{D_1^C, D_2^C, D_3^C\}$ . We set  $D_1^C = \text{NYU}$ ,  $D_2^C = \text{METABRIC}$ , and  $D_3^C = \bigcup\{\text{Korea, Gundersen, Lithuania, BCN, Malaysia, Karmanos, Basel, BASIS, Wales}\}$ .

---

**Algorithm 2** Multiple-source cross-validation for clinical models

---

```
for k = 1 to K do
  for n = 1 to N do
    Sample hyperparameters  $\theta_n$  and train a model  $m_k^{\theta_n}$  using data  $\mathcal{D}^C \setminus D_k^C$ .
  end for
  Select the hyperparameters  $\theta_k^*$  yielding the best overall validation score  $v^{\theta_n}$  for split  $D_k^C$ .
  The model obtained for split  $k$  is  $m_k^{\theta_k^*}$ 
end for
Obtain final model  $m = \frac{1}{K} \sum_1^K m_k^{\theta_k^*}$ 
```

---

### 4.3 The AI model

Our model learns and makes predictions using both clinical variables and digital pathology images. Internally, it is composed of many models whose predictions are ensembled in two rounds. First, the models are ensembled within their data modality. Then, the ensemble of clinical models is combined with the ensemble of digital pathology models. The intuition behind ensembling lies in the idea that different models make errors that are not perfectly correlated. Ensembling several models cancels out some of these errors, adding accuracy and robustness to predictions. An additional advantage of ensembling at the level of modalities is that for every test example, it is easy to interpret the contribution of the clinical data and the digital pathology data to the final prediction.

#### 4.3.1 Creating model ensembles

Ensembling the clinical models happened in two steps. First, the output risk scores from all the clinical models were scaled approximately to the interval  $[0, 1]$ . That is, for each model  $m_k$ , we found the maximum over the entire validation set,  $\max^k = \max_i \{\hat{y}_i^k\}$ , and the minimum over the entire validation set,  $\min^k = \min_i \{\hat{y}_i^k\}$ . For the test examples, the normalized prediction from any model was computed as  $y^k = \frac{\hat{y}^k - \min^k}{\max^k - \min^k}$ . Then predictions from all models were simply averaged. That is, assuming that there were  $K$  models, for any test example, the aggregated clinical prediction was computed as  $y^c = \frac{1}{K} \sum_{k=1}^K y^k$ .

For pathology models, as the predictions already were in the interval  $[0, 1]$ , we simply averaged predictions from different models. That is, for any test example, the aggregated pathology prediction was computed as  $y^p = \frac{1}{K} \sum_1^K y_k^p$ . We generated the final pathology model by averaging the top  $K$  models across different combinations of pooling method (mean, max, or MIL), training loss function (Cox or discrete-time), and feature extractor to form the final ensemble. We used  $K = 10$  for both clinical and pathology models.

Finally, the clinical score and the pathology score were averaged, that is,  $y = \frac{1}{2}(y^c + y^p)$ .

### 4.4 Digital pathology models

Unlike many prior approaches [43, 32, 44], we did not use any hand-crafted pathomic features. Instead, we obtained learned morphological features from Kestrel, our purpose-built foundation model trained on a pan-cancer dataset. These features were used to train time-to-event models. Below we present our model in greater detail.

**Kestrel’s architecture.** Kestrel is a ViT-L which contains 303M parameters. An overview of the vision transformer architecture is provided in Figure 6.

**Preprocessing histopathology slides.** Digital pathology slides are extremely high resolution, often exceeding 1 billion pixels per image. Additionally, large regions of these images are empty. Therefore, to extract only meaningful tissue, we used Otsu’s method [45] to distinguish background from foreground. Subsequently, we patchify the foreground into non-overlapping  $256 \times 256$  patches at  $20\times$  magnification (0.5 microns per pixel). Each slide is thus reduced to a set of patches. There are typically between 8,000 to 16,000 patches per slide.

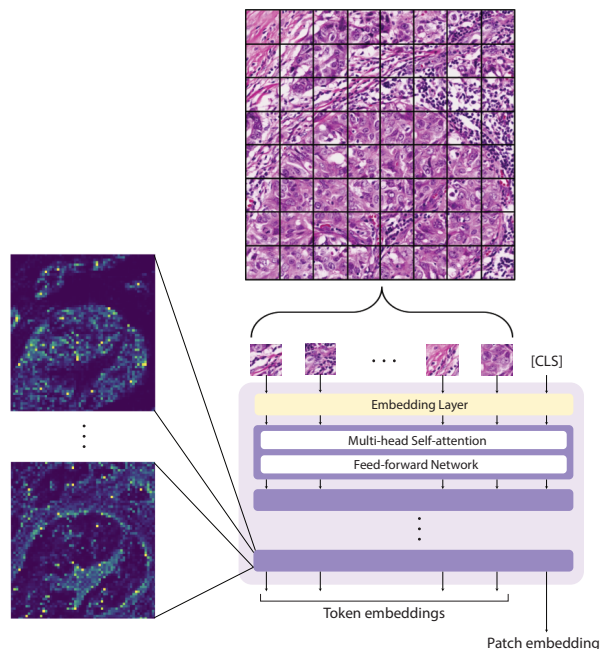


Figure 6: **Overview of the vision transformer (ViT) architecture applied to digital pathology.** Images are first broken into a grid of sub-patches, or “tokens”. These tokens, along with a [CLS] token which serves to aggregate features across sub-patches, are vectorized via an embedding layer. These vectors then progress through a sequence of blocks which consist of multi-headed self-attention followed by a feed-forward network. The ViT output consists of token embeddings and an aggregate patch embedding. The patch embedding is the primary output used downstream, and both the patch and token embeddings are used for self-supervised learning. On the left, we display attention masks between the [CLS] embedding and token embeddings extracted from the final block. These masks provide insight into the types of features the vision transformer is using to create the patch embeddings.

**Training Kestrel.** Kestrel [17] was trained using a self-supervised learning method DINOv2 [13] on 400M patches extracted from 45,000 histopathology slides. We tuned the hyperparameters for training Kestrel by evaluating trained models on a suite of 16 benchmarks. These benchmarks come mostly from public challenges and are designed to test a model’s ability to learn to recognize different characteristics of the micro-tumor environment, for example, tumor cellularity and histology. This has enabled us to train models that excel at generating meaningful features from tissue patches.

**Extracting digital pathology features.** Slides were preprocessed to extract only foreground patches. These foreground patches were passed through our foundation model to obtain patch-level embeddings. These patch-level embeddings are used as an input to a time-to-event model model.

Our model’s predictions were generated using H&E-stained slides from the same tissue block that was previously used for Oncotype DX testing. For an overwhelming majority of the cases (approximately 93% of the patients across all evaluation cohorts), we used only a single slide. For the remaining minority of the cases for which we had more than one slide, we averaged the predictions across slides.

#### 4.4.1 Training the digital pathology models

We trained two types of models using features extracted by Kestrel as input: Cox proportional hazard models and discrete time models.

#### 4.4.2 Cox proportional hazard model

Consider a model,  $m$ , parameterized by  $\beta$ , with the training dataset  $D_T$  and the validation dataset  $D_V$ . The training loss for this model is computed as

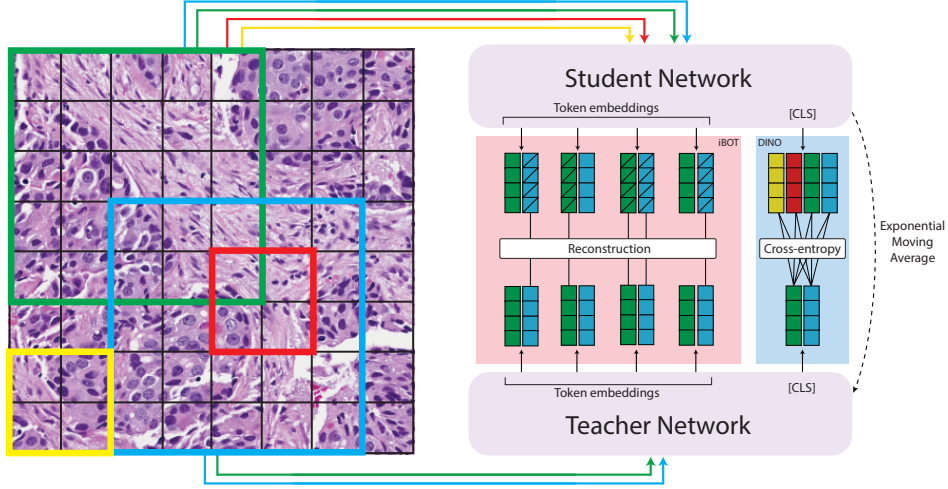


Figure 7: **Overview of self-supervised learning method DINOv2 applied to digital pathology.** First, several larger (global) and smaller (local) crops are sampled from an image and transformed with image augmentations such as blurring, rotation and scaling. Global and local crops are passed through the student network while only global crops are passed through the teacher network. For the DINO loss component, cross-entropy is computed between the student’s CLS token outputs and teacher’s CLS token outputs. For the iBOT loss component, input tokens are randomly masked before passing global crops through the student network, and a reconstruction loss is computed between the corresponding student network token embeddings and the corresponding teacher network token embeddings.

$$\mathcal{L} = (1 - \alpha)\mathcal{L}_{\text{Cox}} + \alpha\mathcal{R}(\beta),$$

where  $\mathcal{L}_{\text{Cox}}$  is the negative log of the partial likelihood computed for the training data,  $\mathcal{R}$  is a regularizer, and  $\alpha$  is a hyperparameter controlling the relative weight of  $\mathcal{L}_{\text{Cox}}$  and  $\mathcal{R}$ .

Specifically, the training loss  $\mathcal{L}_{\text{Cox}}$  is computed as

$$\mathcal{L}_{\text{Cox}} = \frac{1}{|D_T|} \sum_{i \in D_T} \delta_i \log \left( \sum_{j \in \mathcal{S}_i} \exp[g(x_j) - g(x_i)] \right),$$

where  $x_i$  represents image features for a whole slide image,  $g$  is a neural network transforming  $x_i$ ,  $\delta_i$  indicates whether the patient experienced an event, and  $\mathcal{S}_i$  represents the risk set (the individuals that have not yet experienced an event at time  $t_i$ ).

The regularizer  $\mathcal{R}$  is computed as

$$\mathcal{R}(\beta) = \frac{(1 - \gamma)}{2} \|\beta\|_2^2 + \gamma \|\beta\|_1,$$

where  $\gamma$  is a hyperparameter controlling the relative weight of the L1 and L2 regularization terms. The entire training loss is optimized with Adam [46], a variant of stochastic gradient descent.

#### 4.4.3 Discrete-time model

We divide times from  $t_0$  to  $t_J$  into  $J$  contiguous time intervals  $(t_0, t_1], (t_1, t_2], \dots, (t_{J-1}, t_J]$ , where  $t_0 = 0$  and  $t_J = \infty$ .

For subject  $i$  with covariates  $x_i$ , the hazard in interval  $A_j = (t_{j-1}, t_j]$  is

$$\lambda_{ij}(X_i) = \Pr(T_i \in A_j | T_i > t_{j-1}, x_i),$$

and survival probability is then

$$S_i(t|x_i) = \Pr(T_i > t|x_i) = \prod_{j:t_j \leq t} (1 - \lambda_{ij}(x_i)).$$

We introduce an indicator  $d_{ij} = \mathbb{1}[T_i \in A_{ij}] = \mathbb{1}[t_{j-1} < T_i \leq t_j]$ , which for censored subjects is given by  $(d_{i1}, \dots, d_{ij_i}) = (0, \dots, 0)$  and for subjects that experience the event is given by  $(d_{i1}, \dots, d_{ij_i}) = (0, \dots, 0, 1)$ . The likelihood can then be defined as

$$\mathcal{L}_{\text{DT}} = \prod_{i=1}^n \lambda_{ij_i}(x_i)^{d_{ij_i}} \prod_{j=1}^{j_i-1} (1 - \lambda_{ij}(x_i))^{1-d_{ij}},$$

and the log-likelihood is

$$\log \mathcal{L}_{\text{DT}} = \sum_{i=1}^n \left[ d_{ij_i} \log \lambda_{ij_i}(x_i) + \sum_{j=1}^{j_i} (1 - d_{ij}) \log(1 - \lambda_{ij}(x_i)) \right].$$

Then we can model the score at time  $j$  as  $\phi_j(X_i)$ , and to make the hazard between 0 and 1, we set

$$\lambda_{ij}(x_i) = \frac{1}{1 + \exp[-\phi_j(x_i)]}.$$

We can estimate  $\phi_j(x_i)$  by minimizing the negative log-likelihood.

Regularization is added to  $\mathcal{L}_{\text{DT}}$  the same way it is added to  $\mathcal{L}_{\text{Cox}}$  in the previous section.

#### 4.4.4 Aggregation of patch embeddings

In order to train time-to-event neural networks with Cox or discrete-time losses, it is necessary to aggregate patch embeddings into a single vector representation that can be passed into a standard feed-forward neural network. We used two strategies to do this: parameterless pooling and attention-weighted multiple instance learning (MIL) pooling.

**Parameterless pooling.** It has been shown that simple forms of pooling such as mean- and max-pooling perform well on digital pathology tasks where aggregation is needed. Thus, one set of the trained time-to-event models in our pathology ensemble consists of networks trained on mean- or max-pooled patch embeddings with a Cox loss.

**Attention-weighted MIL.** It has also been shown that simple attention-based networks, such as gated attention [47], are also effective ways of aggregating patch embeddings in digital pathology. Thus, we trained a complementary set of time-to-event models using a gated attention network with a discrete-time loss.

## 4.5 Clinical models

For building a model for clinical variables we utilized CatBoost [48], a gradient boosting decision tree ensemble. Its primary advantage over other possible models for this application, e.g., neural networks, is how it handles categorical variables and associated missing values which are inevitable in clinical data. Here, CatBoost is specifically trained with the AFT (accelerated failure time) loss. We utilized AFT models with three potential distributions: normal, logistic, and extreme value.

We used eight routinely collected variables (see Table 2) that characterize breast cancer and are typically used to guide treatment decisions. For instance, ER and PR statuses help determine the tumor’s hormone receptor sensitivity, which is critical for hormone-based therapies. HER2 status is important for targeted therapies like trastuzumab, which is effective in HER2+ cancers.

Table 2: Possible values for the clinical variables used as inputs for our clinical model.

clinical variable	possible values
patient age	[0, 100]
estrogen receptor (ER) status	positive, negative, unknown
progesterone receptor (PR) status	positive, negative, unknown
HER2 biomarker status	positive, negative, equivocal, unknown
T stage (tumor size/extent)	T1mi, T1a, T1b, T1c, T2, T3, T4, TX, unknown
N stage (nodal involvement)	N0, N1, N2, N3, NX, unknown
has IDC component	yes, no, unknown
has ILC component	yes, no, unknown

## References

- [1] S. Paik, S. Shak, G. Tang, C. Kim, J. Baker, M. Cronin, F. L. Baehner, M. G. Walker, D. Watson, T. Park, W. Hiller, E. R. Fisher, L. D. Wickerham, J. Bryant, and N. Wolmark, “A Multigene Assay to Predict Recurrence of Tamoxifen-Treated, Node-Negative Breast Cancer,” *New England Journal of Medicine*, vol. 351, no. 27, pp. 2817–2826, 2004.
- [2] S. Mook, L. J. Van’t Veer, E. J. Rutgers, M. J. Piccart-Gebhart, and F. Cardoso, “Individualization of therapy using Mammaprint: from development to the MINDACT Trial,” *Cancer Genomics Proteomics*, vol. 4, no. 3, pp. 147–155, 2007.
- [3] B. Wallden, J. Storhoff, T. Nielsen, N. Dowidar, C. Schaper, S. Ferree, S. Liu, S. Leung, G. Geiss, J. Snider, T. Vickery, S. Davies, E. Mardis, M. Gnant, I. Sestak, M. J. Ellis, C. M. Perou, P. S. Bernard, and J. S. Parker, “Development and verification of the PAM50-based Prosigna breast cancer gene signature assay,” *BMC Medical Genomics*, vol. 8, no. 1, pp. 1–14, 2015.
- [4] J. A. Sparano, R. J. Gray, D. F. Makower, K. S. Albain, T. J. Saphner, S. S. Badve, L. I. Wagner, V. G. Kaklamani, M. M. Keane, H. L. Gomez, P. S. Reddy, T. F. Goggins, I. A. Mayer, D. L. Toppmeyer, A. M. Brufsky, M. P. Goetz, J. L. Berenberg, C. Mahalcioiu, C. Desbiens, D. F. Hayes, E. C. Dees, J. Geyer, Charles E., J. Olson, John A., W. C. Wood, T. Lively, S. Paik, M. J. Ellis, J. Abrams, and J. Sledge, George W., “Clinical Outcomes in Early Breast Cancer With a High 21-Gene Recurrence Score of 26 to 100 Assigned to Adjuvant Chemotherapy Plus Endocrine Therapy: A Secondary Analysis of the TAILORx Randomized Clinical Trial,” *JAMA Oncology*, vol. 6, no. 3, pp. 367–374, 2020.
- [5] L. J. Esserman, C. Yau, C. K. Thompson, L. J. van ’t Veer, A. D. Borowsky, K. A. Hoadley, N. P. Tobin, B. Nordenskjöld, T. Fornander, O. Stål, C. C. Benz, and L. S. Lindström, “Use of Molecular Tools to Identify Patients With Indolent Breast Cancers With Ultralow Risk Over 2 Decades,” *JAMA Oncology*, vol. 3, no. 11, pp. 1503–1510, 2017.
- [6] L. Pusztai, J. R. Hoag, K. S. Albain, W. E. Barlow, S. M. Stemmer, A. Meisner, G. N. Hortobagyi, S. Shak, D. F. Hayes, J. M. Rae, F. Baehner, P. Sharma, and K. Kalinsky, “Development and validation of RSclin N+ tool for hormone receptor-positive (HR+), HER2-negative (HER2-), node-positive breast cancer.,” *Journal of Clinical Oncology*, 2024.
- [7] F. Miglietta, M. Dieci, T. Giarratano, V. Torri, M. Giuliano, F. Zustovich, M. Mion, C. Tondini, E. Bria, M. Franchi, L. Merlini11, R. Giannatiempo, D. Russo, V. Fotia, P. Poletti, E. R. Caremoli, G. Arpino, G. De Salvo, A. Zambelli, and V. Guarneri, “242MO Association of tumor-infiltrating lymphocytes (TILs) with recurrence score (RS) in patients with hormone receptor-positive (HR+)/HER2-negative (HER2-) early breast cancer (BC): A translational analysis of four prospective multicentric studies,” *Annals of Oncology*, vol. 34, 2023.
- [8] T. Chen, S. Kornblith, M. Norouzi, and G. Hinton, “A Simple Framework for Contrastive Learning of Visual Representations,” in *Proceedings of the 37th International Conference on Machine Learning*, vol. 119 of *Proceedings of Machine Learning Research*, pp. 1597–1607, 2020.

- [9] K. He, H. Fan, Y. Wu, S. Xie, and R. Girshick, “Momentum Contrast for Unsupervised Visual Representation Learning,” in *CVPR*, June 2020.
- [10] J.-B. Grill, F. Strub, F. Altché, C. Tallec, P. Richemond, E. Buchatskaya, C. Doersch, B. Avila Pires, Z. Guo, M. Gheshlaghi Azar, B. Piot, K. Kavukcuoglu, R. Munos, and M. Valko, “Bootstrap your own latent - a new approach to self-supervised learning,” in *Advances in Neural Information Processing Systems*, vol. 33, pp. 21271–21284, 2020.
- [11] K. He, X. Chen, S. Xie, Y. Li, P. Dollár, and R. Girshick, “Masked Autoencoders Are Scalable Vision Learners,” in *CVPR*, pp. 16000–16009, June 2022.
- [12] M. Caron, H. Touvron, I. Misra, H. Jégou, J. Mairal, P. Bojanowski, and A. Joulin, “Emerging Properties in Self-Supervised Vision Transformers,” in *ICCV*, 2021.
- [13] M. Oquab, T. Darcet, T. Moutakanni, H. V. Vo, M. Szafraniec, V. Khalidov, P. Fernandez, D. Haziza, F. Massa, A. El-Nouby, M. Assran, N. Ballas, W. Galuba, R. Howes, P.-Y. Huang, S.-W. Li, I. Misra, M. Rabbat, V. Sharma, G. Synnaeve, H. Xu, H. Jegou, J. Mairal, P. Labatut, A. Joulin, and P. Bojanowski, “DINOv2: Learning Robust Visual Features without Supervision,” *Transactions on Machine Learning Research*, 2024.
- [14] E. Vorontsov, A. Bozkurt, A. Casson, G. Shaikovski, M. Zelechowski, K. Severson, E. Zimmermann, J. Hall, N. Tenenholz, N. Fusi, E. Yang, P. Mathieu, A. van Eck, D. Lee, J. Viret, E. Robert, Y. K. Wang, J. D. Kunz, M. C. H. Lee, J. H. Bernhard, R. A. Godrich, G. Oakley, E. Millar, M. Hanna, H. Wen, J. A. Retamero, W. A. Moye, R. Yousfi, C. Kanan, D. S. Klimstra, B. Rothrock, S. Liu, and T. J. Fuchs, “A foundation model for clinical-grade computational pathology and rare cancers detection,” *Nature Medicine*, 2024.
- [15] R. J. Chen, T. Ding, M. Y. Lu, D. F. K. Williamson, G. Jaume, A. H. Song, B. Chen, A. Zhang, D. Shao, M. Shaban, M. Williams, L. Oldenburg, L. L. Weishaupt, J. J. Wang, A. Vaidya, L. P. Le, G. Gerber, S. Sahai, W. Williams, and F. Mahmood, “Towards a general-purpose foundation model for computational pathology,” *Nature Medicine*, vol. 30, no. 3, pp. 850–862, 2024.
- [16] X. Wang, J. Zhao, E. Marostica, W. Yuan, J. Jin, J. Zhang, R. Li, H. Tang, K. Wang, Y. Li, *et al.*, “A pathology foundation model for cancer diagnosis and prognosis prediction,” *Nature*, pp. 1–9, 2024.
- [17] J. Cappadona, K. G. Zeng, C. Fernandez-Granda, J. Witowski, Y. LeCun, and K. J. Geras, “Squeezing performance from pathology foundation models with chained hyperparameter searches,” in *NeurIPS 2024 Workshop: Self-Supervised Learning - Theory and Practice*, 2024.
- [18] A. Dosovitskiy, L. Beyer, A. Kolesnikov, D. Weissenborn, X. Zhai, T. Unterthiner, M. Dehghani, M. Minderer, G. Heigold, S. Gelly, J. Uszkoreit, and N. Houlsby, “An Image is Worth 16x16 Words: Transformers for Image Recognition at Scale,” in *International Conference on Learning Representations*, 2021.
- [19] K. S. Albain, W. E. Barlow, S. Shak, G. N. Hortobagyi, R. B. Livingston, I.-T. Yeh, P. Ravdin, R. Bugarini, F. L. Baehner, N. E. Davidson, G. W. Sledge, E. P. Winer, C. Hudis, J. N. Ingle, E. A. Perez, K. I. Pritchard, L. Shepard, J. R. Gralow, C. Yoshizawa, D. C. Allred, C. K. Osborne, and D. F. Hayes, “Prognostic and predictive value of the 21-gene recurrence score assay in postmenopausal women with node-positive, oestrogen-receptor-positive breast cancer on chemotherapy: a retrospective analysis of a randomised trial,” *The Lancet Oncology*, vol. 11, no. 1, pp. 55–65, 2010.
- [20] J. A. Sparano, R. J. Gray, D. F. Makower, K. I. Pritchard, K. S. Albain, D. F. Hayes, C. E. Geyer Jr, E. C. Dees, M. P. Goetz, J. A. Olson Jr, *et al.*, “Adjuvant chemotherapy guided by a 21-gene expression assay in breast cancer,” *New England Journal of Medicine*, vol. 379, no. 2, pp. 111–121, 2018.
- [21] K. Kalinsky, W. E. Barlow, J. R. Gralow, F. Meric-Bernstam, K. S. Albain, D. F. Hayes, N. U. Lin, E. A. Perez, L. J. Goldstein, S. K. Chia, *et al.*, “21-gene assay to inform chemotherapy benefit in node-positive breast cancer,” *New England Journal of Medicine*, vol. 385, no. 25, pp. 2336–2347, 2021.

- [22] J. Bartlett, D. Sgroi, K. Treuner, Y. Zhang, I. Ahmed, T. Piper, R. Salunga, E. Brachtel, S. Pirrie, C. Schnabel, and D. Rea, “Breast Cancer Index and prediction of benefit from extended endocrine therapy in breast cancer patients treated in the Adjuvant Tamoxifen—To Offer More?(aTTom) trial,” *Annals of Oncology*, vol. 30, no. 11, pp. 1776–1783, 2019.
- [23] A. Waks, E. Ogayo, L. Paré, M. Marín-Aguilera, F. Brasó-Maristany, P. Galván, O. Castillo, O. Martínez-Sáez, A. Vivancos, P. Villagrasa, G. Villacampa, P. Tarantino, N. Desai, J. Guerriero, O. Metzger, N. M. Tung, I. E. Krop, J. S. Parker, C. M. Perou, A. Prat, E. P. Winer, S. M. Tolaney, and E. A. Mittendorf, “Assessment of the HER2DX Assay in Patients With ERBB2-Positive Breast Cancer Treated With Neoadjuvant Paclitaxel, Trastuzumab, and Pertuzumab,” *JAMA Oncology*, 2023.
- [24] A. Flanagan, T. Frey, and S. L. Christiansen, “Updated Guidance on the Reporting of Race and Ethnicity in Medical and Science Journals,” *JAMA*, vol. 326, no. 7, pp. 621–627, 2021.
- [25] Y. Satpathy, P. Nam, M. Moldovan, J. D. Murphy, L. Wang, I. Derweesh, B. S. Rose, and J. Javier-DesLoges, “Comparison of Capture Rates of the National Cancer Database Across Race and Ethnicity,” *JAMA Network Open*, vol. 6, 12 2023.
- [26] S. Paik, G. Tang, S. Shak, C. Kim, J. Baker, W. Kim, M. Cronin, F. L. Baehner, D. Watson, J. Bryant, J. P. Costantino, C. R. Geyer Jr, D. L. Wickerham, and N. Wolmark, “Gene Expression and Benefit of Chemotherapy in Women With Node-Negative, Estrogen Receptor–Positive Breast Cancer,” *Journal of Clinical Oncology*, vol. 24, no. 23, pp. 3726–3734, 2006.
- [27] M. Takahashi, J. Cortés, R. Dent, L. Pusztai, H. McArthur, S. Kümmel, C. Denkert, Y. H. Park, S.-A. Im, J.-H. Ahn, H. Mukai, C.-S. Huang, S.-C. Chen, M. H. Kim, L. Jia, X. T. Li, K. Tryfonidis, V. Karantza, H. Iwata, and P. Schmid, “Pembrolizumab Plus Chemotherapy Followed by Pembrolizumab in Patients With Early Triple-Negative Breast Cancer: A Secondary Analysis of a Randomized Clinical Trial,” *JAMA Network Open*, vol. 6, no. 11, 2023.
- [28] P. Schmid, J. Cortes, R. Dent, L. Pusztai, H. McArthur, S. Kümmel, J. Bergh, C. Denkert, Y.-K. Park, R. Hui, N. Harbeck, M. Takahashi, M. Untch, P. A. Fasching, F. Cardoso, J. Andersen, D. Patt, M. Danso, M. Ferreira, M.-A. Mouret-Reynier, S.-A. Im, J.-H. Ahn, M. Gion, S. Baron-Hay, J.-F. Boileau, Y. Ding, K. Tryfonidis, G. Aktan, V. Karantza, and J. O’Shaughnessy, “Event-free Survival with Pembrolizumab in Early Triple-Negative Breast Cancer,” *The New England Journal of Medicine*, vol. 386, no. 6, pp. 556–567, 2022.
- [29] C. A. Santa-Maria, “Optimizing and Refining Immunotherapy in Breast Cancer,” *JCO Oncology Practice*, vol. 19, no. 4, pp. 190–191, 2023.
- [30] S. Tolaney, K. Ballman, C. M. Perou, D. Cescon, M. Gatti-Mays, V. Blinder, S. Rosenberg, E. Mittendorf, A. Weiss, H. Rugo, A. Ho, D. Casey, B. Singh, F. Smieliauskas, Y. Abdou, V. Damarla, J. Meisel, L. Carey, and A. Partridge, “OptimICE-pCR: De-escalation of therapy in early-stage TNBC patients who achieve pCR after neoadjuvant chemotherapy with checkpoint inhibitor therapy (Alliance A012103) [abstract],” in *Proceedings of the 2023 San Antonio Breast Cancer Symposium*, vol. 84, AACR, 2024.
- [31] S. R. Stecklein, A. Aripoli, R. Salgado, A. O’Dea, L. E. Nye, K. E. Larson, D. Satelli, R. Rader, R. Madan, R. Yoder, J. M. Staley, I. Fernandez, A. Heinrich, J. L. Wagner, C. Balanoff, L. Kilgore, L. Bantis, A. K. Godwin, Q. J. Khan, and P. Sharma, “NeoTRACT: Phase II trial of neoadjuvant tumor infiltrating lymphocyte- and response-adapted chemoimmunotherapy for triple-negative breast cancer (TNBC),” *Journal of Clinical Oncology*, vol. 42, no. 16-suppl, 2024.
- [32] G. Fernandez, M. Prastawa, A. S. Madduri, R. Scott, B. Marami, N. Shpalensky, K. Cascetta, M. Sawyer, M. Chan, G. Koll, A. Shtabsky, A. Feliz, T. Hansen, B. Veremis, C. Cordon-Cardo, J. Zeineh, and M. J. Donovan, “Development and validation of an AI-enabled digital breast cancer assay to predict early-stage breast cancer recurrence within 6 years,” *Breast Cancer Research*, vol. 24, no. 1, pp. 1–11, 2022.
- [33] D. E. Spratt, S. Tang, Y. Sun, H.-C. Huang, E. Chen, O. Mohamad, A. J. Armstrong, J. D. Tward, P. L. Nguyen, J. M. Lang, J. Zhang, A. Mitani, J. P. Simko, S. DeVries, D. van der Wal, H. Pinckaers, J. M.

- Monson, H. A. Campbell, J. Wallace, M. J. Ferguson, J.-P. Bahary, E. M. Schaeffer, H. M. Sandler, P. T. Tran, J. P. Rodgers, A. Esteva, R. Yamashita, and F. Y. Feng, “Artificial Intelligence Predictive Model for Hormone Therapy Use in Prostate Cancer,” *NEJM Evidence*, vol. 2, no. 8, 2023.
- [34] D. E. Spratt, Y. Sun, D. Van der Wal, S.-C. Huang, O. Mohamad, A. J. Armstrong, J. D. Tward, P. Nguyen, E. Chen, S. DeVries, J. M. Monson, H. A. Campbell, M. J. Ferguson, J.-P. Bahary, P. T. Tran, J. P. Rodgers, A. Esteva, and F. Y. Feng, “An AI-derived digital pathology-based biomarker to predict the benefit of androgen deprivation therapy in localized prostate cancer with validation in NRG/RTOG 9408,” *Journal of Clinical Oncology*, 2022.
- [35] I. Garberis, V. Gaury, C. Saillard, D. Drubay, K. Elugi, B. Shumauch, A. Jaeger, L. Herpin, J. Linhart, M. Sapaterio, F. Berginole, A. Kamoun, E. Bendjebbar, A. de Lavergne, R. Dubois, M. Auffret, L. Guillou, I. Bousaid, M. Azoulay, J. Lemonnier, M. Sefta, A. Jacquet, A. Sarrazin, J. Reboud, F. Brulport, J. Dachary, B. Pistilli, S. Delalogue, P. Courtiol, F. André, V. Aubert, and M. Lacroix-Triki, “Deep Learning Allows Assessment of Risk of Metastatic Relapse from Invasive Breast Cancer Histological Slides,” *bioRxiv*, 2022.
- [36] S. Volinsky-Fremont, N. Horeweg, S. Andani, J. Barkey Wolf, M. W. Lafarge, C. D. de Kroon, G. Ørtoft, E. Høgdaal, J. Dijkstra, J. J. Jobsen, L. C. H. W. Lutgens, M. E. Powell, L. R. Mileshekin, H. Mackay, A. Leary, D. Katsaros, H. W. Nijman, S. M. de Boer, R. A. Nout, M. de Bruyn, D. Church, V. T. H. B. M. Smit, C. L. Creutzberg, V. H. Koelzer, and T. Bosse, “Prediction of recurrence risk in endometrial cancer with multimodal deep learning,” *Nature Medicine*, vol. 30, pp. 1962–1973, 7 2024.
- [37] The Cancer Genome Atlas Network, “Comprehensive molecular portraits of human breast tumours,” *Nature*, vol. 490, no. 7418, pp. 61–70, 2012.
- [38] G. Ciriello, M. L. Gatza, A. H. Beck, M. D. Wilkerson, S. K. Rhie, A. Pastore, H. Zhang, M. McLellan, C. Yau, C. Kandoth, R. Bowlby, H. Shen, S. Hayat, R. Fieldhouse, S. C. Lester, G. M. Tse, R. E. Factor, L. C. Collins, K. H. Allison, Y.-Y. Chen, K. Jensen, N. B. Johnson, S. Oesterreich, G. B. Mills, A. D. Cherniack, G. Robertson, C. Benz, C. Sander, P. W. Laird, K. A. Hoadley, T. A. King, and C. M. Perou, “Comprehensive molecular portraits of invasive lobular breast cancer,” *Cell*, vol. 163, no. 2, pp. 506–519, 2015.
- [39] C. Curtis, S. P. Shah, S.-F. Chin, G. Turashvili, O. M. Rueda, M. J. Dunning, D. Speed, A. G. Lynch, S. Samarajiwa, Y. Yuan, S. Graf, G. Ha, G. Haffari, A. Bashashati, R. Russell, S. McKinney, M. Group, A. Langerød, A. R. Green, E. Provenzano, G. Wishart, S. Pinder, P. Watson, F. Markowitz, L. Murphy, I. Ellis, A. Purushotham, A.-L. Borresen-Dale, J. D. Brenton, S. Tavare, C. Caldas, and S. Aparicio, “The genomic and transcriptomic architecture of 2000 breast tumours reveals novel subgroups,” *Nature*, vol. 486, no. 7403, 2012.
- [40] S. Nik-Zainal, H. Davies, J. Staaf, M. Ramakrishna, D. Glodzik, X. Zou, I. Martincorena, L. B. Alexandrov, S. Martin, D. C. Wedge, P. Van Loo, Y. S. Ju, M. Smid, A. B. Brinkman, S. Morganella, M. R. Aure, O. C. Lingjærde, A. Langerød, M. Ringnér, S.-M. Ahn, S. Boyault, J. E. Brock, A. Broeks, A. Butler, C. Desmedt, L. Dirix, S. Dronov, A. Fatima, J. A. Foekens, M. Gerstung, G. K. J. Hooijer, S. J. Jang, D. R. Jones, H.-Y. Kim, T. A. King, S. Krishnamurthy, H. J. Lee, J.-Y. Lee, Y. Li, S. McLaren, A. Menzies, V. Mustonen, S. O’Meara, I. Pauporté, X. Pivot, C. A. Purdie, K. Raine, K. Ramakrishnan, F. G. Rodríguez-González, G. Romieu, A. M. Sieuwerts, P. T. Simpson, R. Shepherd, L. Stebbings, O. A. Stefansson, J. Teague, S. Tommasi, I. Treilleux, G. G. Van den Eynden, P. Vermeulen, A. Vincent-Salomon, L. Yates, C. Caldas, L. van’t Veer, A. Tutt, S. Knappskog, B. K. T. Tan, J. Jonkers, A. Borg, N. T. Ueno, C. Sotiriou, A. Viari, P. A. Futreal, P. J. Campbell, P. N. Span, S. Van Laere, S. R. Lakhani, J. E. Eyfjord, A. M. Thompson, E. Birney, H. G. Stunnenberg, M. J. van de Vijver, J. W. M. Martens, A.-L. Børresen-Dale, A. L. Richardson, G. Kong, G. Thomas, and M. R. Stratton, “Landscape of somatic mutations in 560 breast cancer whole-genome sequences,” *Nature*, vol. 534, no. 7605, pp. 47–54, 2016.
- [41] J. Bergstra and Y. Bengio, “Random Search for Hyper-Parameter Optimization,” *Journal of Machine Learning Research*, vol. 13, no. 10, 2012.

- [42] K. Geras and C. Sutton, “Multiple-source cross-validation,” in *Proceedings of the 30th International Conference on Machine Learning*, vol. 28 of *Proceedings of Machine Learning Research*, 2013.
- [43] M. Amgad, J. M. Hodge, M. A. Elsebaie, C. Bodelon, S. Puvanesarajah, D. A. Gutman, K. P. Siziopikou, J. A. Goldstein, M. M. Gaudet, L. R. Teras, and L. A. Cooper, “A population-level digital histologic biomarker for enhanced prognosis of invasive breast cancer,” *Nature Medicine*, vol. 30, no. 1, pp. 85–97, 2024.
- [44] V. Nimgaonkar, V. Krishna, V. Krishna, E. Tiu, A. Joshi, D. Vrabac, H. Bhambhvani, K. Smith, J. S. Johansen, S. Makawita, *et al.*, “Development of an artificial intelligence-derived histologic signature associated with adjuvant gemcitabine treatment outcomes in pancreatic cancer,” *Cell Reports Medicine*, vol. 4, no. 4, 2023.
- [45] N. Otsu, “A Threshold Selection Method from Gray-Level Histograms,” *IEEE Transactions on Systems, Man, and Cybernetics*, vol. 9, no. 1, 1979.
- [46] D. P. Kingma and J. Ba, “Adam: A Method for Stochastic Optimization.,” in *ICLR*, 2015.
- [47] M. Ilse, J. Tomczak, and M. Welling, “Attention-based deep multiple instance learning,” in *International conference on machine learning*, pp. 2127–2136, PMLR, 2018.
- [48] L. Prokhorenkova, G. Gusev, A. Vorobev, A. V. Dorogush, and A. Gulin, “Catboost: unbiased boosting with categorical features,” *Advances in Neural Information Processing Systems*, vol. 31, 2018.
- [49] F. E. Harrell, R. M. Califf, D. B. Pryor, K. L. Lee, and R. A. Rosati, “Evaluating the Yield of Medical Tests,” *JAMA*, vol. 247, no. 18, pp. 2543–2546, 1982.
- [50] N. Mantel, “Evaluation of survival data and two new rank order statistics arising in its consideration,” *Cancer Chemotherapy Reports*, vol. 50, no. 3, pp. 163–170, 1966.
- [51] G. Schwarzer, “meta: An R Package for Meta-Analysis,” *R news*, vol. 7, no. 3, pp. 40–45, 2007.

## Data availability

TCGA-BRCA data can be accessed from The Cancer Imaging Archive under doi:10.7937/K9/TCIA.2016.AB2NAZRP. The BASIS dataset can be requested from the Wellcome Sanger Institute and was accessed from the European Genome-Phenome Archive (EGA) under accession number EGAS00001001178. The METABRIC dataset can be requested from the METABRIC Committee and was accessed from EGA under accession number EGAD00010000270. The remaining datasets are private or proprietary and are not publicly available.

## Code availability

The model can be accessed for non-commercial research. We have also documented all experiments with sufficient details in our Methods section to enable independent replication. Although the codebase cannot be shared due to its proprietary nature, the core components of our work rely on open-source repositories:

- DINOv2 model architecture for self-supervised training:
  - <https://github.com/facebookresearch/dinov2>
- PyTorch library for training and inference:
  - <https://github.com/pytorch/pytorch>
- For preprocessing whole slide images:
  - OpenSlide: <https://openslide.org>
  - wsidicom: <https://github.com/imi-bigpicture/wsidicom>

- For training and models for survival analysis:
  - CatBoost: <https://github.com/catboost/catboost>
  - PyCox: <https://github.com/havakv/pycox>
  - Scikit-learn: <https://github.com/scikit-learn/scikit-learn>
  - Torch Tuples: <https://github.com/havakv/torch tuples>
- For result analysis:
  - NumPy: <https://github.com/numpy/numpy>
  - Metagen: <https://cran.r-project.org/web/packages/meta/meta.pdf>
  - Lifelines: <https://github.com/CamDavidsonPilon/lifelines>
  - Concordance: <https://cran.r-project.org/web/packages/survival/vignettes/concordance.pdf>
- For visualizations:
  - Seaborn: <https://github.com/mwaskom/seaborn>
  - Matplotlib: <https://github.com/matplotlib/matplotlib>

## Acknowledgements

DZP acknowledges funding from the Research Council of Lithuania (LMTLT), agreement No. S-PD-22-86. For METABRIC cohort: This study makes use of data generated by the Molecular Taxonomy of Breast Cancer International Consortium. Funding for the project was provided by Cancer Research UK and the British Columbia Cancer Agency Branch. For TCGA-BRCA cohort: The results shown here are in whole or part based upon data generated by the TCGA Research Network: <http://cancergenome.nih.gov/>. For Wales cohort: Biosamples were obtained from the Wales Cancer Bank (doi:10.5334/ojb.46) which is funded by Health and Care Research Wales. Other investigators may have received specimens from the same subjects. For Breast Cancer Now Biobank cohort: The authors wish to acknowledge the roles of the Barts Cancer Now Tissue Bank in collecting and making available the samples and/or data, and the patients who have generously donated their tissues and shared their data to be used in the generation of this publication.

## Author contributions

JW and KJG contributed to study conception. CFG, LP, YLC and KJG contributed as research advisors. NC, FS, UO, VS, LMP, NK, AB and FJE provided clinical guidance. JW, KZ, JC and KL wrote code, developed infrastructure and trained models throughout the study. JW, KZ, JC, JE, EDC, YJK, FH, ZS, NT, MS, FY, EL, TH, BS, DR, AC, VS, MV, LS, SMS, DB, KC, YZ, LD, AS, WA, RB, JWP, HM, SHT, VA, DZP, AL, BDP, CB, SYJ, JPY, SHL and KJG worked on data preparation. JW, KZ, JC, IO, CFG and KJG performed evaluation and analysis. IO contributed as a statistical advisor. JW, KZ, JC, IO, CFG and KJG worked on drafting and revising the manuscript. All authors critically reviewed the paper and the results and approved the final version.

## Competing interests

JW, KZ, JC, CFG, FS, ZS, AB, FJE, YLC and KJG are equity holders of Ataraxis AI. IO served as a consultant for Ataraxis AI. New York University (NYU) maintains financial and intellectual property interests in Ataraxis AI that are pertinent to the research presented in this manuscript. JW and KJG are inventors on a US patent filed corresponding to some of the methodological aspects of this work. The remaining authors declare no competing interests.

# A Appendix

## A.1 Concordance index

C-index, originally proposed by Harrell et al. [49], is a metric of accuracy for time-to-event models, analogous to AUROC for classification, adjusted for the possibility of censoring. It is defined as the ratio of the number of *concordant* pairs of test examples to the number of all *comparable* pairs of test examples. A test example is defined by its event time,  $T$ , its vector of input features,  $x$ , and  $\delta$  indicating the presence of an event. Two test examples are comparable if the example with the shorter event time is not censored (i.e., experienced an event). Two test examples are concordant if the model assigns a higher risk score to the example with the shorter event time. Given  $\delta_i = 1$  indicating the presence of an event and  $T_i$  the ‘time-to-event’ response for example  $i$ , we use Equation 1 to compute the C-index:

$$C = \frac{\sum_{i,j} [\text{risk}(x_i) > \text{risk}(x_j)] \cdot [T_i < T_j] \cdot \delta_i}{\sum_{i,j} [T_i < T_j] \cdot \delta_i}. \quad (1)$$

## A.2 Hazard ratio

Hazard ratio is a metric appropriate for measuring how well a model can divide patients into two groups, e.g. low- and high-risk. The hazard ratio is computed using the Cox proportional hazards model, in which the input indicates one of the two groups. That is, we model the hazard for an individual at time  $t$  as  $\lambda(t|x) = \lambda_0(t) \exp(\beta x)$ , where  $x$  is the group indicator ( $x = 0$  or  $x = 1$ ),  $\lambda_0(t)$  is the baseline hazard function which represents the hazard when  $x = 0$  and  $\beta$  is the regression coefficient associated with the variable indicating the group a patient belongs to. Then, based on the data, this model is fitted using partial likelihood. For the fitted model, hazard ratio is computed as

$$\text{HR} = \frac{\lambda(t|x=1)}{\lambda(t|x=0)} = \frac{\lambda_0(t) \exp(\beta \cdot 1)}{\lambda_0(t) \exp(\beta \cdot 0)} = \exp(\beta).$$

If  $\text{HR} > 1$ , the group with  $x = 1$  has a higher hazard of experiencing the event in comparison to the group with  $x = 0$ . If  $\text{HR} < 1$ , the group with  $x = 0$  has a higher hazard of experiencing the event in comparison to the group with  $x = 1$ . For example, if  $\text{HR} = 0.5$  the risk for the group with  $x = 0$  is twice the risk for the group with  $x = 1$ .

Hazard ratio can be analogously defined for a continuous  $x$ . Then, it is interpreted as the change in the hazard associated with a one-unit increase in  $x$ . That is,

$$\text{HR} = \frac{\lambda(t|x=\alpha+1)}{\lambda(t|x=\alpha)} = \frac{\lambda_0(t) \exp(\beta \cdot (\alpha+1))}{\lambda_0(t) \exp(\beta \cdot \alpha)} = \exp(\beta).$$

Additionally, the logrank test [50] is commonly utilized to determine if there the hazard ratio is significantly different from one between two groups. The Wald test is utilized to assess the significance of individual predictors or the hazard ratio for a specific variable within a multivariate Cox model.

## A.3 Random effects model

When comparing metrics across different datasets, a random effects model can be applied to account for the variability between these datasets. The random effects model accounts for both within-dataset variability (the inherent variation in the evaluated metric within each dataset) and between-dataset variability (differences between the datasets themselves).

The random effects model takes the following form

$$M_i = \mu + u_i + \epsilon_i,$$

where  $M_i$  is the metric for dataset  $i$ ,  $\mu$  is the overall effect,  $u_i$  is the random effect for dataset  $i$  ( $u_i \sim \mathcal{N}(0, \tau^2)$ ,  $\tau^2$  represents the variance between datasets) and  $\epsilon_i$  is the within-data-set noise ( $\epsilon_i \sim \mathcal{N}(0, \sigma^2)$ ,  $\sigma^2$  represents within-data-set variance). The overall fixed effect  $\mu$  provides a summary of the model’s average performance across datasets. The model is fit using maximum likelihood, as implemented in the Metagen package [51].

## A.4 Endpoint definitions

Table 3: Endpoint definitions and applicable events (local recurrence, distant recurrence, and death from any causes).

endpoint	local-regional re- currence	distant recurrence	death (any cause)
overall survival (OS)			✓
disease-free interval (DFI)	✓	✓	
distant recurrence-free interval (DRFI)		✓	
recurrence-free survival (RFS)	✓	✓	✓
distant recurrence-free survival (DRFS)		✓	✓

## A.5 Multivariate Cox analyses

Multivariate analysis was conducted to assess the significance of the pathology model adjusted for the clinical model (see Table 4), importance of AI test after adjusting for datasets (see Table 6), and AI test after adjusting for various additional factors (see Table 6).

Table 4: Cox multivariate analysis was performed across all test sets, evaluating the hazard ratio associated with the clinical and pathology model scores with DFI as the outcome. Separate analyses were conducted for the entire patient cohort and for the subset of patients with Oncotype scores. Dataset indicator variables were included to adjust for differences between datasets.

	All patients	Oncotype only
Events	279	67
Total	3502	858
Clinical	1.86 (1.67-2.07, p=0.00)	1.58 (1.21-2.06, p=0.00)
Pathology	2.35 (1.51-3.66, p=0.00)	8.82 (3.30-23.53, p=0.00)
Chicago dataset	0.48 (0.27-0.84, p=0.01)	0.34 (0.18-0.62, p=0.00)
Karmanos dataset	1.12 (0.60-2.08, p=0.73)	0.89 (0.47-1.70, p=0.72)
Nightingale dataset	0.67 (0.44-1.04, p=0.07)	-
TCGA dataset	0.50 (0.30-0.84, p=0.01)	-

Table 5: Cox multivariate analysis was conducted across all test sets, evaluating the hazard ratios associated with the AI test with Disease-Free Interval (DFI) as the primary outcome. Dataset-specific indicators were included to adjust for inter-dataset variability in outcomes.

	All patients	Patients with Oncotype	Oncotype intermediate risk
Events	279	67	39
Total	3502	858	526
AI Test	3.63 (2.99-4.40, p=0.00)	3.46 (2.16-5.54, p=0.00)	3.45 (1.85-6.42, p=0.00)
Chicago dataset	0.49 (0.28-0.87, p=0.01)	0.43 (0.24-0.77, p=0.00)	0.41 (0.19-0.90, p=0.03)
Karmanos dataset	1.16 (0.63-2.15, p=0.63)	1.19 (0.64-2.22, p=0.58)	1.65 (0.76-3.57, p=0.21)
Nightingale dataset	0.69 (0.45-1.06, p=0.09)	-	-
TCGA dataset	0.55 (0.34-0.89, p=0.01)	-	-

## A.6 Forest plots for all endpoints

Complete results for both primary and exploratory endpoints are available, with C-index shown in Figure 8 and hazard ratios shown in Figure 9. These results include our model’s performance across various endpoints,

Table 6: Cox multivariate analysis was conducted across all test sets with Oncotype scores, evaluating the hazard ratios associated with the AI test, cancer grade, age, and race, with Disease-Free Interval (DFI) as the primary outcome. Separate analyses were performed with and without the inclusion of the AI score. Dataset-specific indicators were included to adjust for inter-dataset variability in outcomes. To ensure a fair comparison of hazard ratios, we scale both AI test score and Oncotype to a common range of [0-5]. Oncotype, originally on a 0-100 scale, is divided by 20, while our score, on a 0-1 scale, is multiplied by 5.

	with AI test	without AI test
AI Test	-	3.11 (1.91-5.09, p=0.00)
grade	1.38 (0.89-2.14, p=0.15)	1.24 (0.80-1.94, p=0.34)
Race: Other/Unknown	0.64 (0.21-1.94, p=0.43)	0.72 (0.24-2.16, p=0.56)
Race: Asian	0.43 (0.06-3.22, p=0.41)	0.37 (0.05-2.77, p=0.33)
Race: Black	1.15 (0.57-2.32, p=0.70)	1.22 (0.61-2.45, p=0.58)
Oncotype	1.76 (1.12-2.77, p=0.01)	1.47 (0.93-2.30, p=0.10)
Chicago dataset	0.24 (0.07-0.80, p=0.02)	0.30 (0.09-1.00, p=0.05)
Karmanos dataset	0.81 (0.31-2.14, p=0.67)	0.91 (0.35-2.41, p=0.85)

the performance of the model on individual datasets along with pooled outcomes derived from a random effects model.

### A.7 Forest plots for clinically relevant subgroups

Complete results different subgroups are available for the primary endpoint of DFI, with C-index shown in Figure 10 and hazard ratios shown in Figure 11. These results include our model’s performance across various endpoints, the performance of the model on individual datasets, along with pooled outcomes derived from a random effects model.

### A.8 Forest plots for the independent performance of Oncotype DX and the AI test

Full results from the random effects model comparing Oncotype and AI test performance, evaluated in patients with Oncotype scores, are available in Figure 12

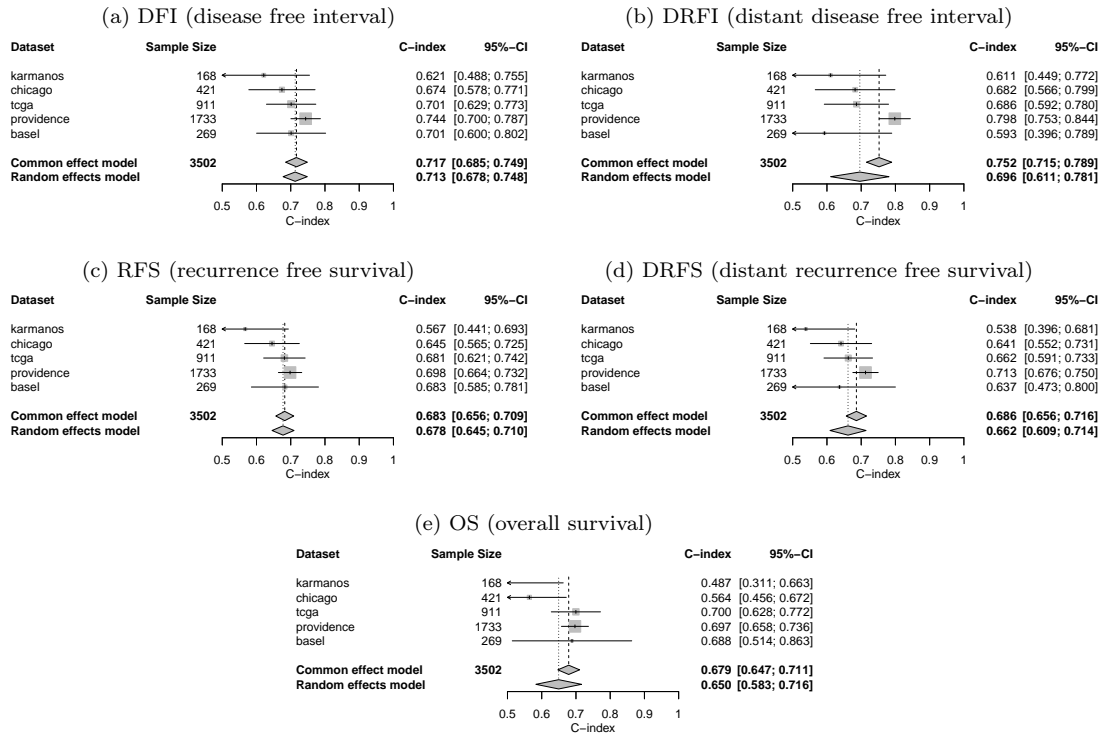


Figure 8: Random effect models for aggregating C-index based on continuous AI score for secondary endpoints.

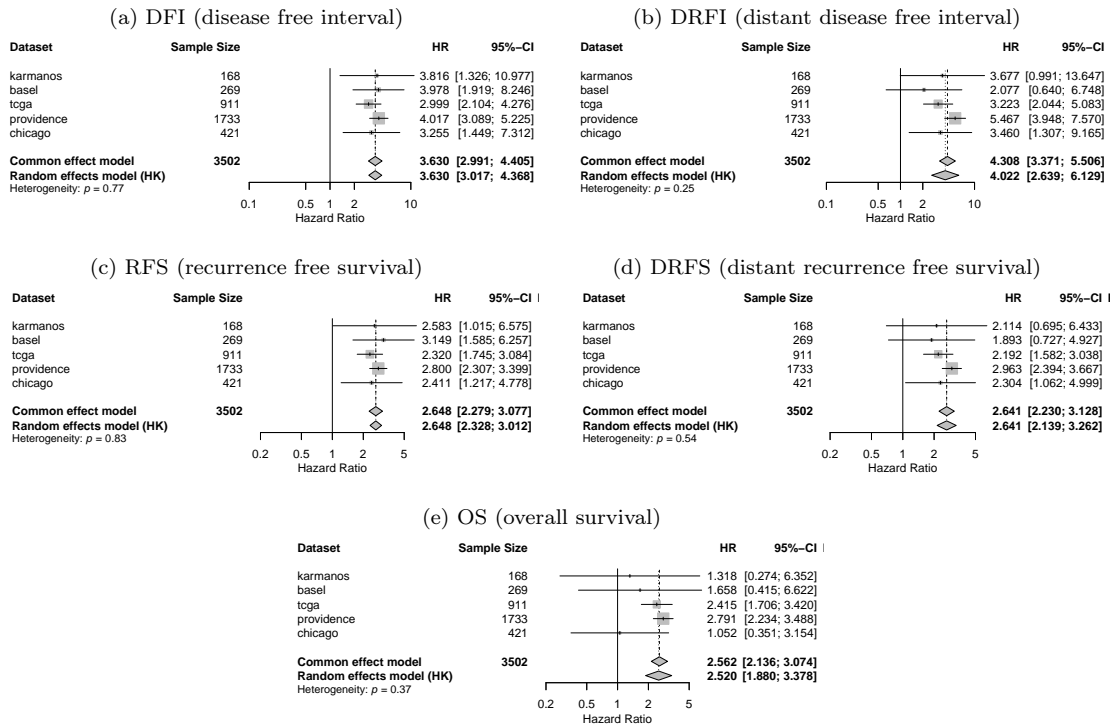


Figure 9: Random effect models for aggregating hazard ratios based on continuous AI score for secondary endpoints.

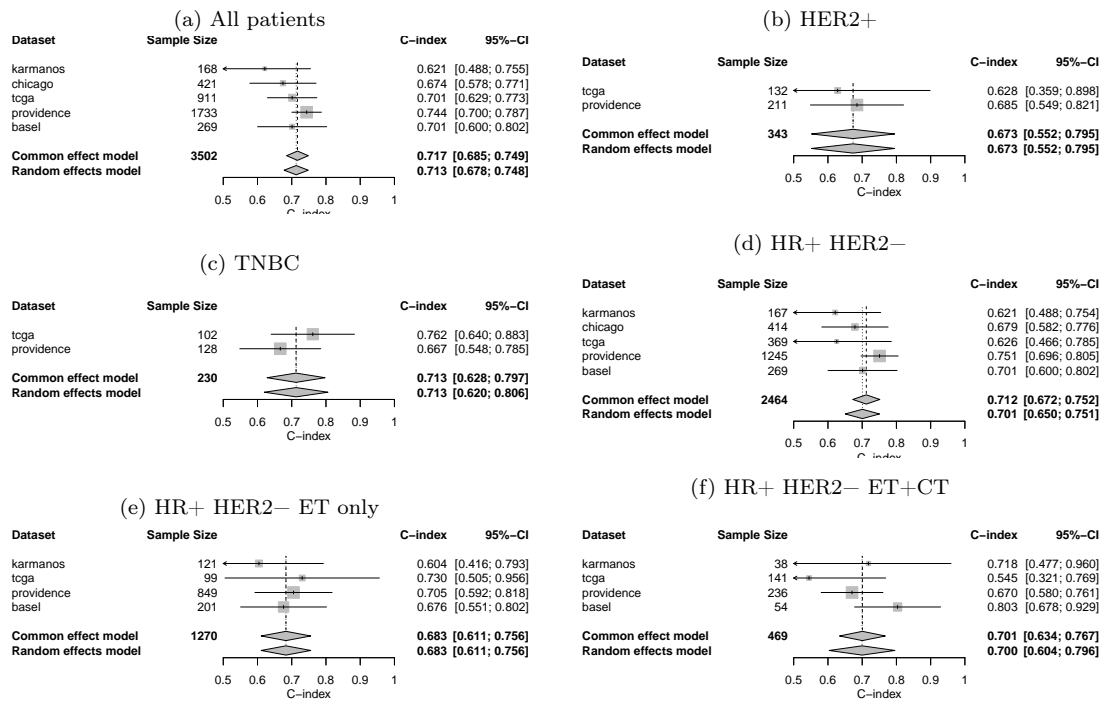


Figure 10: Random effect models for aggregating C-index based on continuous AI score for different patient subgroups.

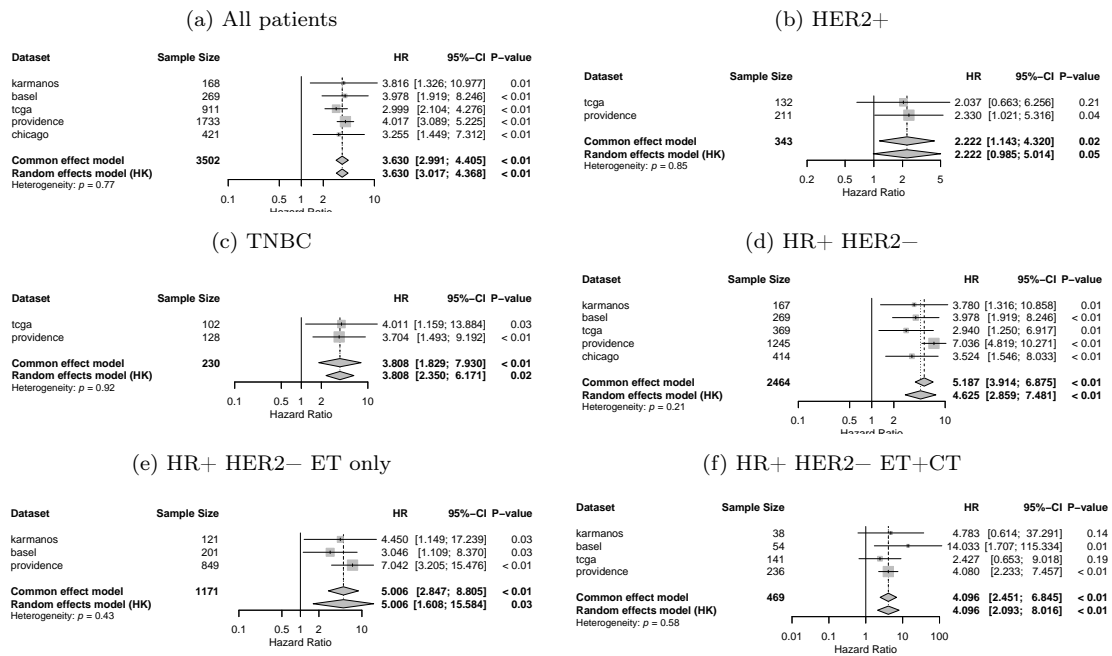


Figure 11: Random effect models for aggregating hazard ratios based on continuous AI score for different patient subgroups.

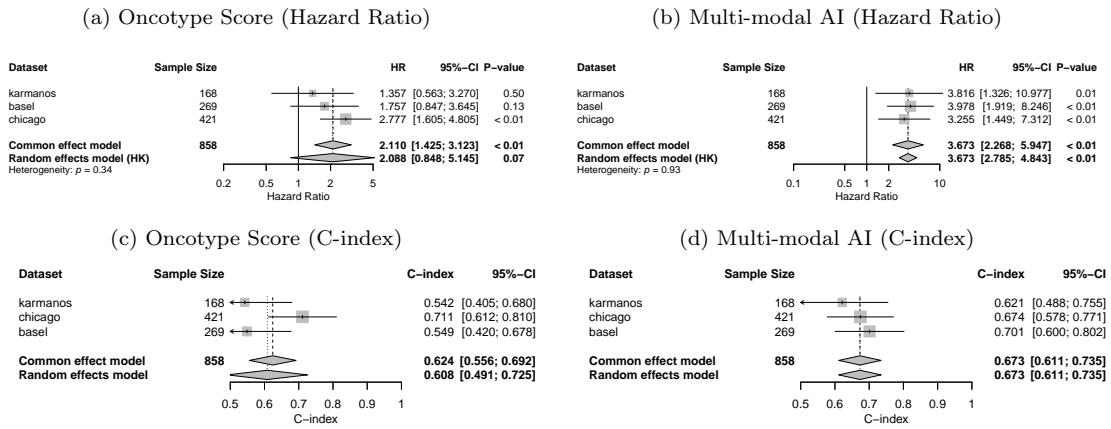


Figure 12: Random effect models for comparing the hazard ratios between Oncotype and the AI test for the primary DFI endpoint.